2

Integral Fast Reactor
Integral Fast Reactor
Integral Fast Reactor
Integral Fast Reactor
Integral Fast Reactor
Integral Fast Reactor
Integral Fast Reactor
Integral Fast Reactor
Integral Fast Reactor
Integral Fast Reactor
Integral Fast Reactor
Integral Fast Reactor
Integral Fast Reactor
Integral Fast Reactor
Integral Fast Reactor
Integral Fast Reactor
Integral Fast Reactor
Integral Fast Reactor
Integral Fast Reactor
Integral Fast Reactor
Integral Fast Reactor
Integral Fast Reactor
Integral Fast Reactor
Integral Fast Reactor
Integral Fast Reactor
Integral Fast Reactor
Integral Fast Reactor
Integral Fast Reactor
Integral Fast Reactor
Integral Fast Reactor
Integral Fast Reactor

ANL-IFR-152

IFR

# Fuel/Cladding Compatibility in Low-Burnup U-26Pu-10Zr/HR9 Fuel at Elevated Temperatures

by Hanchung Tsai, Da-Yung Wang,
F. E. Savoie, and A. G. Hins

Argonne National Laboratory, Argonne, Illinois 60439
operated by The University of Chicago
for the United States Department of Energy under Contract W-31-109-Eng-38

**IFR Technical Memorandum**
Res~~ults reported in the IFR-TM series~~ of me~~moranda frequently are preliminary~~ and subject to revision. Consequently they should not be quoted or referenced.

~~**Applied Technology**~~
Any further distribution by any holder of this document or data therein to third parties ~~representing foreign interests, foreign gov-~~ernments, foreign companies, and foreign ~~subsidiaries or foreign divisions of U.S.~~ companies shall be approved by the Associate Deputy Assistant Secretary for Reactor ~~Systems Development and Technology, U.S.~~ Department of Energy. Further, foreign party releas~~e may require DOE approval pursuant~~ to Federa~~l Regulation 10 CFR Part 810, and/or~~ may be subject to Section 127 of the Atomic Energy Act.

Released for announcement in NAT.
~~Distribution limited to participants~~
~~in the LMFBR program. Others request~~
from RSDT, DOE.

## DISCLAIMER

September 1991 ANL-IFR-152

# FUEL/CLADDING COMPATIBILITY IN LOW-BURNUP U-26Pu-10Zr/HT9 FUEL AT ELEVATED TEMPERATURES

by

Hanchung Tsai, Da-Yung Wang, F. E. Savoie, and A. G. Hins

Materials and Components Technology
Argonne National Laboratory
9700 South Cass Avenue
Argonne, IL 60439

IFR TECHNICAL MEMORANDUM NO. 152

R~~esults reported in~~ the IFR ~~TM series of memo~~randa f~~requently are prel~~iminary a~~nd subject to revi~~sion. C~~onsequently they sh~~ould not ~~be quoted or referen~~ced.

~~APPLIED TECHNOLOGY~~

Any further distri~~bution by any holder of this~~ document or data therein to third parties representing foreign interests, foreign governments, forei~~gn companies, and foreign subsi~~diaries or foreign divisions of U.S. companies shall be approved by the Associate Deputy Assistant S~~ecretary for Reactor Systems,~~ Development, and Tech~~nology, U.S. Depar~~tment of Energ~~y. Further, forei~~gn party rel~~ease may require DOE~~ approval pursu~~ant to Federal Regu~~lation 10 CFR ~~Part 810, and/or m~~ay be subject ~~to Section 127 of t~~he Atomic Energy Act.

MASTER

Releas~~ed for announcement in~~ NAT. Sa
Distrib~~ution limited to participa~~nts
in the ~~LMFBR program. Other~~s request
from RSDT, DOE.

# TABLE OF CONTENTS

Page

ABSTRACT .......... vii

I. INTRODUCTION .......... 1

II. EXPERIMENTAL .......... 1

- A. Test Apparatus .......... 1
- B. Test Pin and Specimens .......... 2
- C. Test Procedure .......... 6
- D. Test Matrix .......... 8

III. RESULTS .......... 10

- A. Temperature for Onset of Liquid-Phase Formation .......... 10
- B. Changes in Fuel and Cladding Structures .......... 10
- C. Cladding Penetration Rates .......... 16
  - 1. As a Function of Temperature .......... 16
  - 2. As a Function of Time .......... 16
- D. Fuel Behavior during NRC Bounding Event 1B .......... 22

IV. DISCUSSION .......... 35

- A. Effects of Pu Content in Fuel .......... 35
- B. Penetration at the Onset of Heating .......... 36
- C. Fuel Compaction .......... 36
- D. Long-duration Test Potential with the FBTA .......... 36

V. SUMMARY .......... 37

VI. ACKNOWLEDGMENTS .......... 38

VII. REFERENCES .......... 38

APPENDIX: CONDITION OF AS-IRRADIATED T678 PIN BEFORE FBTA TESTING... 40

- A. Summary of HFEF NDE and Gas Sampling Results .......... 40
- B. Summary of Metallographic Examination Results .......... 43

## LIST OF FIGURES

Page

1. Schematic Diagram of the Fuel Behavior Test Apparatus .......... 3
2. Assembly Drawing for X430 Pin T678 .......................... 5
3. Transverse Section of Pin T678 at X/L = 0.77 after Steady-state Irradiation .......................................... 7
4. Example of Temperature Control Capability of FBTA ............. 8
5. Transverse Section of 90-18 Test Specimen after 1 h at 750°C ... 11
6. Transverse Section of 90-17 Test Specimen after 1 h at 800°C ... 12
7. Solidified Structure of Once-liquefied Fuel .................. 14
8. Liquid-phase-fuel/Cladding Interaction in 90-17 Specimen ....... 15
9. Effective Cladding Penetration Rates for Specimens Tested for 1.0 h .............................................. 17
10. Transverse Section of 90-19 Test Specimen after 5 min at 800°C 18
11. Transverse Section of 90-21 Test Specimen after 2 h at 800°C ... 19
12. Typical Fuel/Cladding Interaction Zones in 90-21 Specimen ...... 20
13. Time-dependent Cladding Penetration at 800°C .................. 21
14. Thermal History of 90-24 Test Simulating NRC Bounding Event 1B . 23
15. Transverse Section of 90-22 Specimen after Simulated 0.40$ UTOP Event (2 min at 815°C) ..................................... 24
16. Transverse Section of 90-20 Specimen after Simulated 0.40$ UTOP and 9.3-h Hold at 700°C .................................... 25
17. Transverse Section of 90-23 Specimen after Simulated 0.40$ UTOP and 16.6-h Hold at 700°C ................................... 26
18. Transverse Section of 90-24 Specimen after Simulated 0.40$ UTOP and 36-h Hold at 700°C .................................... 27
19. Comparison of Fuel/Cladding Interaction in Test Specimens (a) 90-22, (b) 90-20, and (c) 90-24 .......................... 28

LIST OF FIGURES (Contd.)

Page

20. Cladding Penetration during Simulated NRC Bounding Event 1B .... 29

21. Fuel/Cladding Interaction Zone in 90-24 Test Specimen .......... 30

22. Outline of Area Examined with Scanning Electron Microscope ..... 31

23. BSE Image of Outlined Area in Fig. 22 .......................... 32

24. BSE Image of Interface Region between Areas B and C, Showing Grain-Boundary Structure in Area B and Stringers in Area C ..... 34

A1. Neutron Radiographs of T678 Pin at Two Different Exposures ..... 41

A2. Contact Profilometry Trace of Pin T678, Showing Negligible Cladding Strain ........................................... 42

A3. Transverse Section of Pin T678 at X/L = 0.20 (M1) after Steady-state Irradiation ....................................... 45

A4. Transverse Section of Pin T678 at X/L = 0.49 (M2) after Steady-state Irradiation ....................................... 46

A5. Transverse Section of Pin T678 at X/L = 0.91 (M4) after Steady-state Irradiation ....................................... 47

A6. Fission-product Accumulations in As-irradiated Fuel ........... 48

A7. As-irradiated Pin T678 Cladding, Showing No Obvious Fuel/Cladding Interaction ....................................... 49

LIST OF TABLES

Page

I. Nominal Design Parameters of T678 Pin .......................... 4

II. U-26Pu-10Zr/HT9 Test Matrix ................................... 9

III. SEM/EDX Compositions (at.%) of Fuel/Cladding Interface Zones in FBTA 90-24 Specimen ......................................... 31

# FUEL/CLADDING COMPATIBILITY IN LOW-BURNUP U-26Pu-10Zr/HT9 FUEL AT ELEVATED TEMPERATURES

by

Hanchung Tsai, Da-Yung Wang, F. E. Savoie, and A. G. Hins

## ABSTRACT

A series of out-of-pile fuel/cladding compatibility tests was conducted on EBR-II-irradiated U-26wt.%Pu-10wt.%Zr fuel specimens with HT9 cladding to support PRISM Advanced Liquid Metal Reactor (ALMR) fuel development. Burnup of the test specimens was 2.3 at.%, the highest available from the EBR-II irradiation program at the time of testing. The test temperatures ranged from 700 to 815°C and the test durations ranged from 2 min to 36 h. Following the tests, the specimens were metallographically examined and the extent of fuel/cladding interaction was determined. Results showed that the interaction between the U-26Pu-10Zr fuel and the HT9 cladding at high temperature resulted in liquid-phase penetration into the cladding, and at the same time, liquefaction of the fuel periphery. The interaction mechanism was similar to that of the lower-Pu fuel/HT9 cladding systems previously tested. In terms of the onset-of-liquid-phase-formation temperature and cladding penetration rates, the performance of the test specimens was comparable to that of the other metallic fuel systems. The compatibility behavior was apparently not affected by the higher Pu content in the fuel. In tests simulating an extremely severe transient (NRC bounding event 1B), that lasted up to 36 h at 700°C, the results indicated slow cladding penetration ($\approx 3$ µm/h) and minimal fuel liquefaction.

# I. INTRODUCTION

PRISM (Power Reactor-Innovative Small Modules)[1] is an advanced liquid-metal-cooled fast reactor design that features enhanced reactor safety, fuel cycle economics, and environmental protection. These advantages are, to a large extent, the direct results of using a metallic U-Pu-Zr alloy as the fuel material.[1-3]

The U and Pu constituents in the fuel, however, have a propensity for interacting metallurgically with the stainless steel cladding.[4-5] During steady-state irradiation, solid-state interdiffusion may occur across the fuel/cladding interface. If the fuel pin is then subjected to a high-temperature off-normal reactor event, the interdiffusion layers may begin to liquefy, thus dissolving additional fuel and causing liquid-phase penetration into the cladding. Such interaction can potentially reduce fuel-pin lifetime and result in cladding breach.

To assess the effects of such interactions on the reliability of PRISM fuel pins, a series of out-of-pile fuel/cladding compatibility tests was conducted. The test specimens were obtained from a preirradiated EBR-II pin with prototypical materials for the current PRISM fuel design (U-26wt.%Pu-10wt.%Zr fuel and HT9 cladding). This pin, at a peak burnup of 2.3 at.%, was the first preirradiated U-26Pu-10Zr/HT9 pin available from the EBR-II IFR irradiation program. When higher-burnup U-26Pu-10Zr/HT9 pins are available, similar compatibility tests will be conducted to assess the burnup effects.

# II. EXPERIMENTAL

## A. Test Apparatus

All tests in this series were conducted in the Fuel Behavior Test Apparatus (FBTA)[6] located in the Alpha-Gamma Hot Cell Facility (AGHCF) at Argonne National Laboratory in Illinois. A quad-elliptical radiant furnace, powered by four longitudinal infrared filaments, provided isothermal heating of the test specimen. Shaped and highly reflective surfaces behind the filaments focused the radiant energy onto the centerline of the furnace where the specimen was located. The test specimens were short segments of the irradiated fuel pin placed inside a slightly taller tantalum cup. A single bare-wire Pt/Pt-Rh thermocouple welded onto the outside of the specimen cup monitored the specimen temperature. The output from the thermocouple was used to regulate, via a microcomputer and a feedback algorithm, the furnace power for achieving the desired test temperature. Because of the negligible thermal inertia of the infrared filaments and the strong focusing of the radiant energy, heat-up of the specimen to the desired test temperature typically took less than ≈40 s. The temperature lag between the thermocouple and the fuel specimen during the heat-up was small (≤30°C) and disappeared almost immediately once the steady-state test temperature was reached.[7] Because heat was provided to the specimen externally, no significant radial temperature gradient existed in the fuel or the cladding at the test temperature. During the steady-state portion of the test, temperature fluctuation was typically less than ±2°C.

The specimen in the FBTA was separated from the nitrogen hot-cell atmosphere by two concentric quartz tubes. A high-purity helium purge flow in the inner quartz tube provided an inert atmosphere to protect the test specimen at temperature.

A schematic diagram showing the specimen and the radiant furnace is given in Fig. 1. A detailed description of the FBTA can be found in Ref. 6.

## B. Test Pin and Specimens

The specimens used in the tests were obtained from an EBR-II irradiated pin, T678. This pin had U-26wt.%Pu-10wt.%Zr fuel, 75% planar fuel smear density, a 343-mm-long fuel column, 7.37 mm-OD, 0.42 mm-wall HT9 cladding, and a sodium bond. The nominal design parameters of the pin are shown in Table I, and the assembly drawing is shown in Fig. 2.

The T678 pin was irradiated in a corner position in subassembly X430A in EBR-II from runs 150 through 152. At the time of discharge, peak fuel burnup was 2.3 at.%. The beginning-of-life (BOL) peak linear power and cladding ID temperature were 11.5 kW/m and 555°C, respectively.

Nondestructive examination (NDE) of the pin and plenum-gas sampling and analysis were performed at the Hot Fuel Examination Facility (HFEF). The results, presented in the Appendix, showed no unusual features. The overall condition of the pin was judged to be excellent.

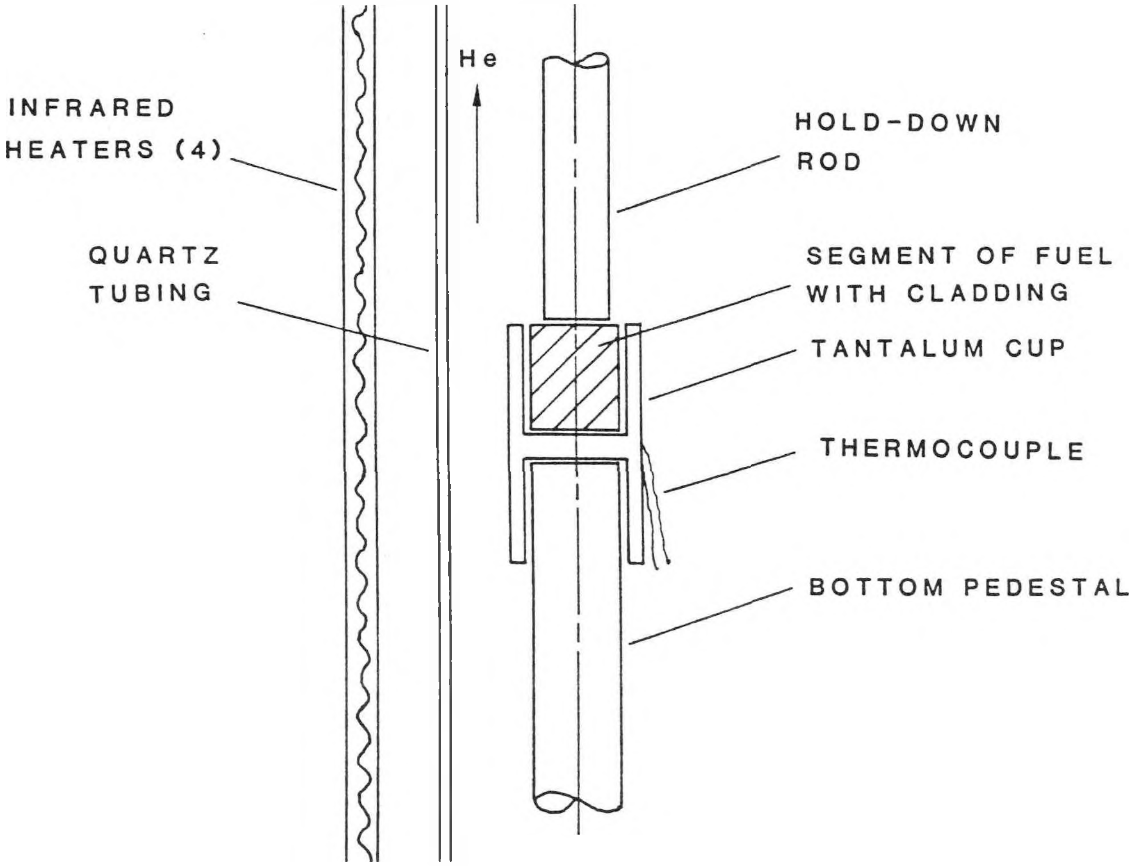

Fig. 1. Schematic Diagram of the Fuel Behavior Test Apparatus

Four transverse sections, from axial locations of X/L = 0.20, 0.48, 0.77 and 0.91, were metallographically examined at the AGHCF to determine the internal condition of the fuel pin after the irradiation. In addition to serving as a benchmark for assessing changes caused by the high-temperature FBTA testing, the data were also of importance to the steady-state irradiation program. (Pin T678 was the first and only U-26Pu-10Zr/HT9 pin discharged at the time.) In the metallographic examination,

Table I. Nominal Design Parameters of T678 Pin

| | |
|---|---|
| Pin Diameter | 0.290 in. (7.37 mm) |
| Cladding Material | HT9 |
| Cladding Thickness | 0.0165 in. (0.42 mm) |
| Fuel Material | U-26wt.%Pu-10wt.%Zr |
| $^{235}$U Enrichment ($^{235}$U/Total U) | 15.5 wt.% |
| Fuel Slug Diameter | 0.223 in. (5.67 mm) |
| Fuel Slug Density | 15.8 g/ml (100% TD) |
| Fuel/cladding Diametral Gap | 0.034 in. (0.86 mm) |
| Planar Fuel Smear Density | 75% |
| Fuel Column Height | 13.5 in. (343 mm) |
| Fuel Column Weight | 139 g |
| Upper or Lower Blanket | None |
| Fuel/Cladding Bond | Sodium |
| Nominal Bond (BOL, at room temp.) | 0.25 in. above fuel |
| Plenum Length (BOL, at room temp.) | 14.5 in. (373 mm) |
| Plenum/Fuel Volume Ratio (BOL) | 1.5 |
| Plenum Gas | 75% He + 25% Ar |
| Gas Tag | Yes |
| TED's | No |
| Fuel Hold-down Spring | No |
| Overall Pin Length | 29.75 in. (749 mm) |
| End Plug Material | HT9 |
| Spacer Wire Diameter | 0.056 in. (1.067 mm) |
| Wire Material | HT9 |
| Pitch-to-diameter Ratio | 1.28 |
| Axial Wire-wrap Pitch | 6 in. (152 mm) |
| Wire Tension | 6.0 lb |
| Pitch Orientation | Clockwise |

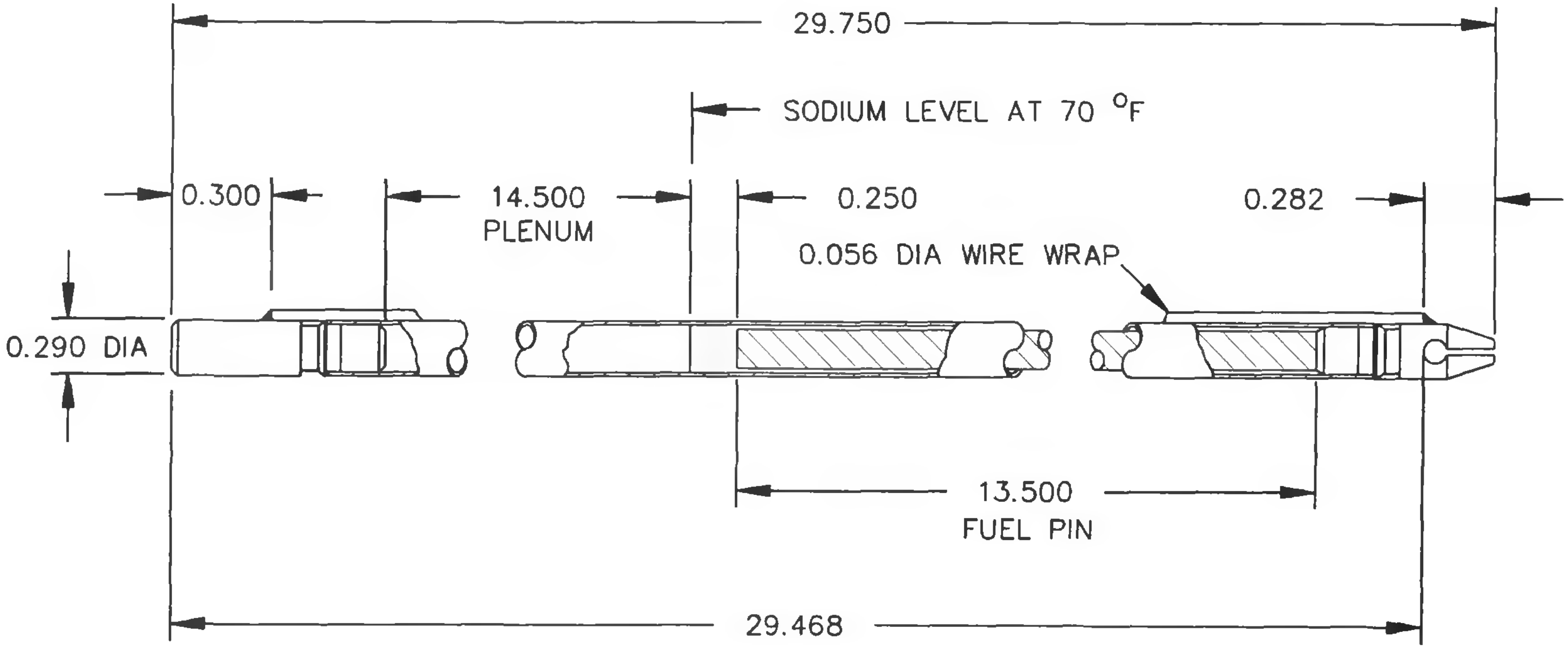

ALL DIMENSIONS IN inches

05966

Fig. 2. Assembly Drawing for X430 Pin T678

the fuel pin was found to be in excellent condition. Fuel/cladding interdiffusion during the steady-state irradiation was apparently minor because little sign of interaction could be detected on the cladding ID. The results of the metallographical examination of the steady-state samples are given in the Appendix. With the X/L = 0.77 section, shown in Fig. 3, used as an example, the key features noted in the examination were (1) closed fuel/cladding gap, (2) distinct zone formation in the fuel due to the redistribution of U and Zr, (3) a wedge-shaped crack in the fuel periphery from the anisotropic swelling of the fuel early-in-life, and (4) little noticeable solid fission-product accumulation on or near the fuel surface. All of these features were expected.

The test specimens, each a ≈7-mm long segment of the fuel pin, were prepared by transverse cutting with an abrasive saw with no lubricants. The ends of the specimens were ground square to facilitate length measurements and visual inspection. To retard specimen oxidation in the AGHCF nitrogen atmosphere ($\leq$250 ppm oxygen), the specimens were kept in individually sealed vials until used for testing.

All specimens used in the FBTA testing were obtained from the same section of the pin, between X/L = 0.66 to 0.84. The purpose of selecting specimens from a close proximity was to minimize possible axial variation of the condition of the fuel, either from the fuel-slug casting process or from irradiation.

### C. Test Procedure

Prior to each test, the desired test conditions, along with the proper trip settings, were programmed into the control computer. Trips were set to minimize the risk to the hot cell from malfunctioning of components in the FBTA. The desired test duration was entered into the control program to facilitate an automatic shutoff of the furnace power at the conclusion of a test.

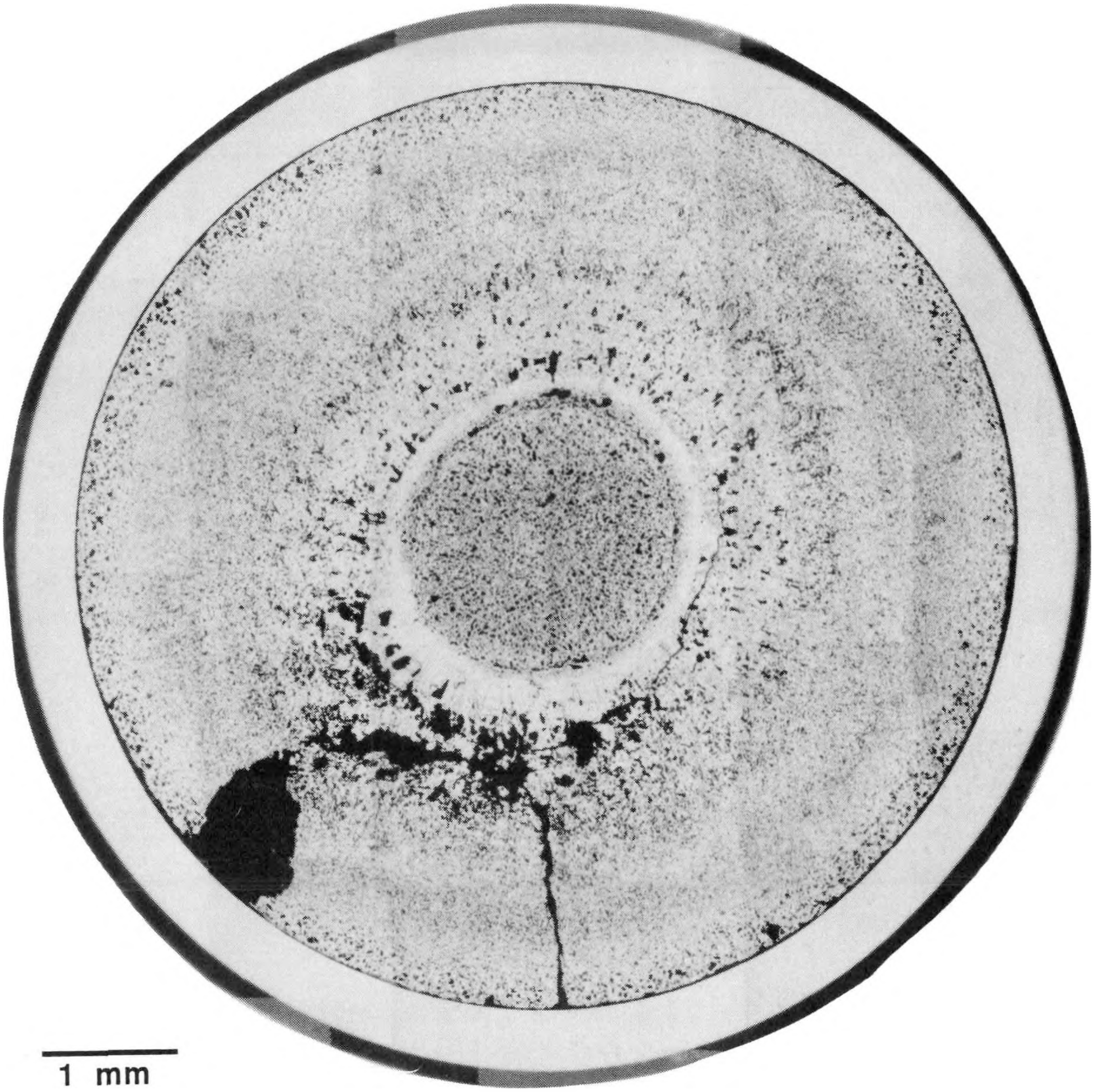

Fig. 3. Transverse Section of Pin T678 at X/L = 0.77 after Steady-state Irradiation (As-polished, MCT 277592)

After the specimen was loaded in the FBTA, the helium gas flow was turned on for several minutes to purge the test chamber. The furnace was then powered up by executing the temperature/power control program. Following the shutdown, the specimen was allowed to cool by radiant and convective heat losses. Figure 4 illustrates the attained temperature history of a typical test.

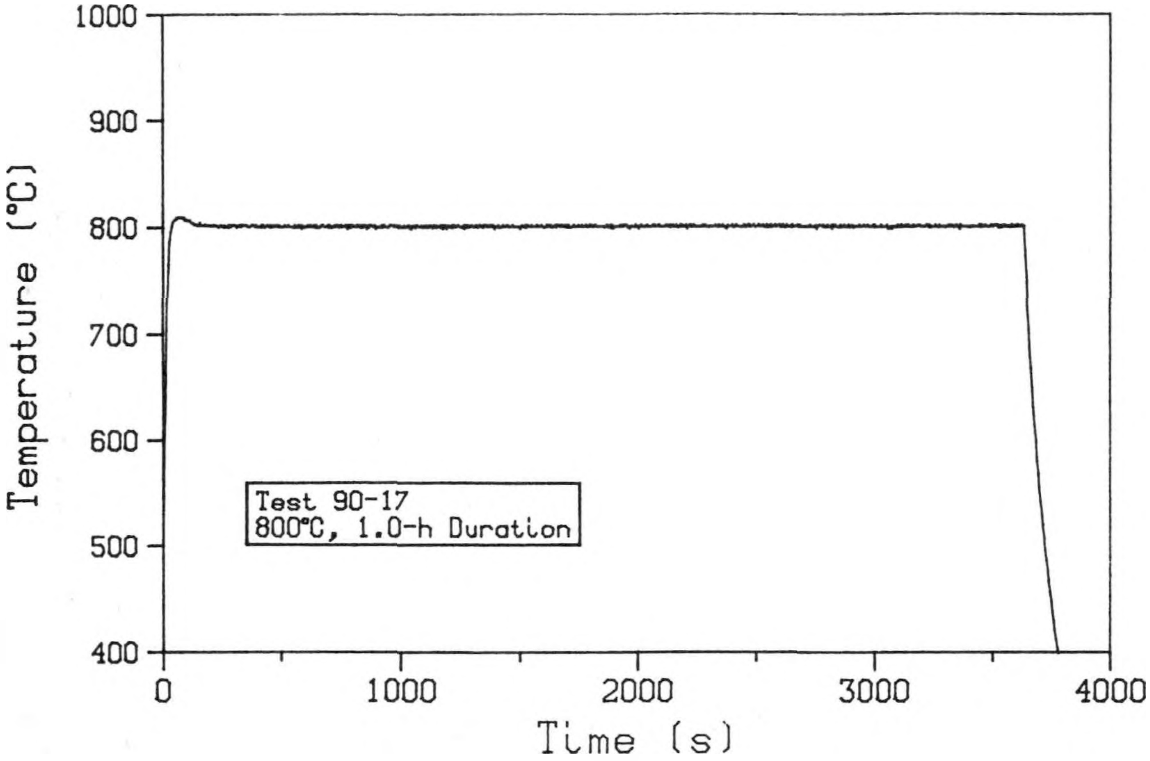

Fig. 4. Example of Temperature Control Capability of FBTA. This was actual test condition for Test 90-17 in this series.

After each test, the specimen was metallographically examined in the AGHCF. The examination was typically made on a transverse section near the axial midplane of the specimen. Evidence of fuel surface liquefaction and cladding interaction was determined in the examination. From high-magnification photomicrographs, the maximum depth of cladding penetration was determined by comparing the thickness of the as-built cladding and that of the thinnest remaining cladding in the circumference.

## D. Test Matrix

The test series consisted of eight tests. The key parameters of the tests are shown in Table II. Four of the tests, 90-17, -18, -19, and -21, were constant-temperature, fixed-duration tests; they were designed to yield data on the temperature for the onset of liquid-phase formation and rates of cladding penetration. The data, when compared with the existing FBTA test data base, highlight performance differences between the PRISM-type fuels and the other metallic fuel types previously tested.

The remaining four tests in this series (90-20, -22, -23, and -24) were designed to yield data on PRISM fuel behavior during the NRC bounding event 1B. This event, consisting of a 0.40$ unterminated transient overpower (UTOP) and a concurrent loss of intermediate heat transfer system (IHTS), has the highest severity among essentially all unscrammed transients for the ALMR. (A detailed description of this event can be found in Ref. 1.) In these tests, it was simulated by a 2-min flattop at 815°C, followed by a hold of up to 36-h at 700°C.

Table II. U-26Pu-10Zr/HT9 Test Matrix

| FBTA Test No. | Specimen No. | Axial Loc. (X/L) | Test Temp. ($^{o}$C) | Test Duration |
|---|---|---|---|---|
| 90-17 | A/G 409A11 | 0.80 | 800 | 1.0 h |
| 90-18 | A/G 409A12 | 0.82 | 750 | 1.0 h |
| 90-19 | A/G 409A13 | 0.84 | 800 | 5.0 min |
| 90-20 | A/G 409A14 | 0.86 | a | 9.3 h |
| 90-21 | A/G 409A7 | 0.88 | 800 | 2.0 h |
| 90-22 | A/G 409A18 | 0.66 | 815 | 2.0 min |
| 90-23 | A/G 409A17 | 0.69 | b | 16.6 h |
| 90-24 | A/G 409A15 | 0.74 | c | 36.0 h |

[a] 815$^{o}$C for 2 min, followed by 700$^{o}$C for 9.3 h.
[b] 815$^{o}$C for 2 min, followed by 700$^{o}$C for 16.6 h.
[c] 815$^{o}$C for 2 min, followed by 700$^{o}$C for 36.0 h.

## III. RESULTS

### A. Temperature for Onset of Liquid-Phase Formation

The temperature for the onset of liquid-phase formation is defined as the minimum temperature above which readily detectable liquid phases, due to fuel/cladding interaction, would form within 1 h.*

This temperature for the U-26Pu-10Zr/HT9 test fuel was bracketed in the 90-17 and 90-18 tests. In the 750°C 90-18 test, the specimen incurred no noticeable fuel liquefaction or liquid-phase cladding attack, as shown in Fig. 5. On the other hand, the 800°C 90-17 test specimen clearly showed fuel liquefaction and liquid-phase cladding penetration (Fig. 6). The temperature for the onset of liquid-phase-formation was thus determined to be between 750 and 800°C. This temperature is slightly better than the 725-750°C found previously for the other metallic fuel systems.[8]

### B. Changes in Fuel and Cladding Structures

The high-temperature treatment of the test specimens in the FBTA induced noticeable changes in the condition of the fuel and fuel/cladding interface. A general description of these changes in fuel and cladding microstructures is provided in this section, based on the results from the 90-17 and 90-18 tests.

---

*The selection of 1 h for this purpose was based on two practical considerations:

(1) This duration encompasses essentially all of the postulated terminated and unterminated off-normal reactor events.[9] Thus, if no liquefaction is detected in the FBTA in 1 h, it is unlikely that liquefaction would occur in a reactor in a shorter transient. To address the few specific reactor events with longer durations, designated tests (such as the 90-20, -23, -24 tests in this series) are conducted.

(2) This duration is convenient from the standpoint of FBTA operation and has been used since the beginning of the current compatibility testing program. It thus provides a consistent basis for comparing the performances of various metallic fuel/cladding systems.

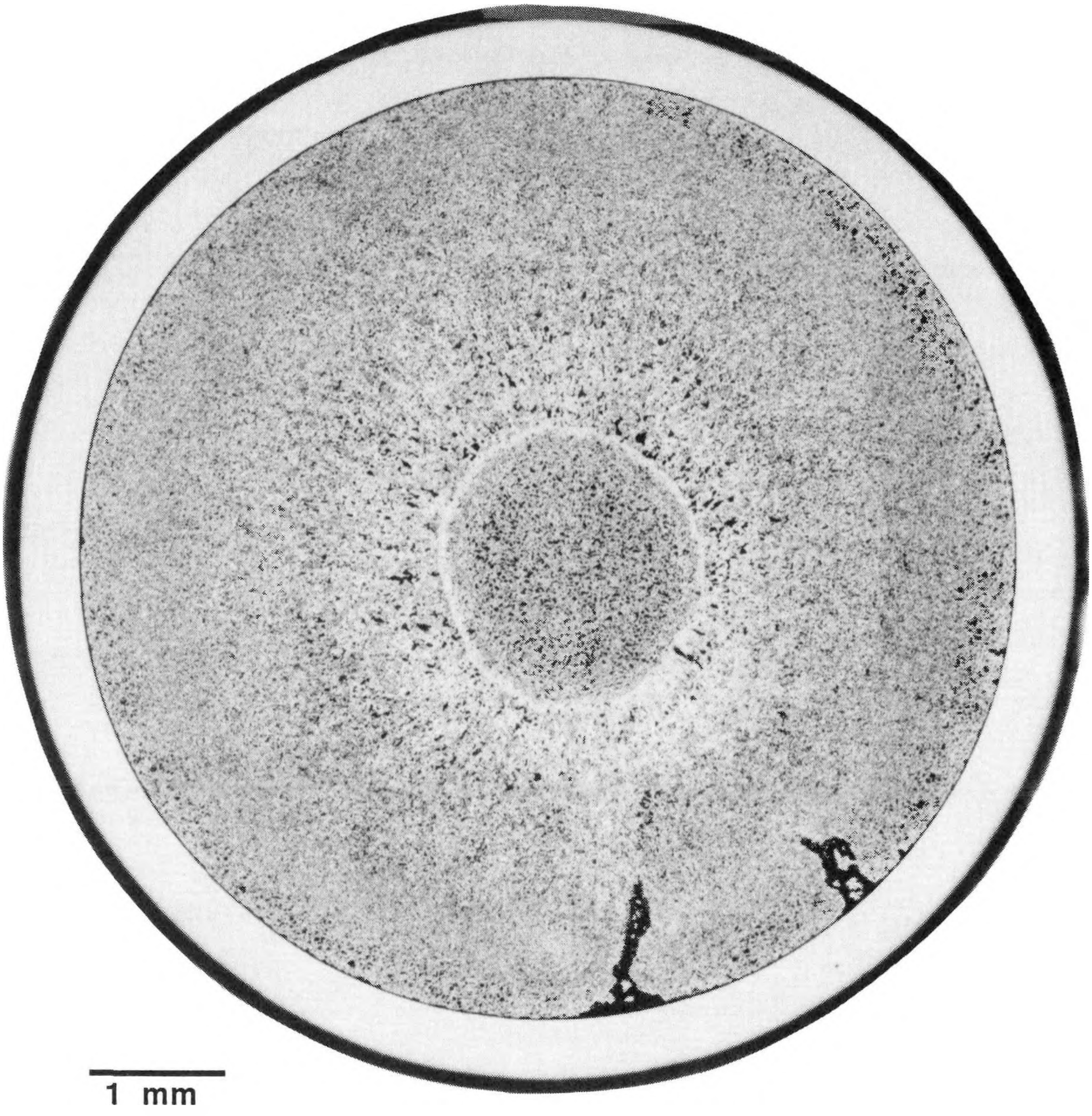

Fig. 5. Transverse Section of 90-18 Test Specimen after 1 h at 750°C. There are noticeable changes in fuel structure (cf. Fig. 3) due to the test, but no signs of fuel/cladding interaction. (As-polished, MCT 277872).

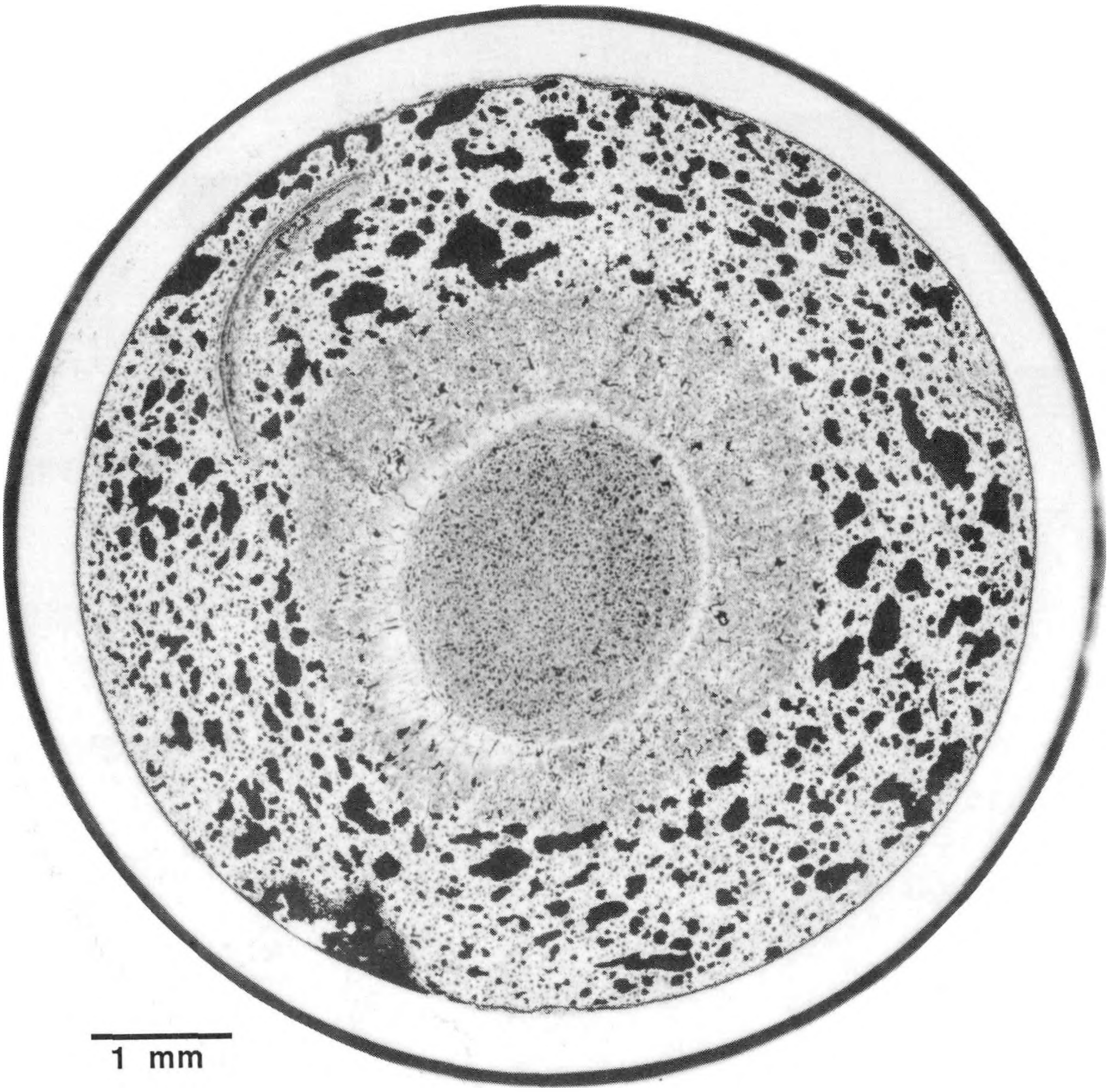

Fig. 6. Transverse Section of 90-17 Test Specimen after 1 h at 800°C. Fuel liquefaction extended to approximately mid-radius. Arc-shaped structure in ten-o'clock direction is probably an artifact from casting. (As-polished, MCT 277871)

In the 750°C 90-18 test, even though there was no liquid-phase fuel/cladding interaction, substantial fuel restructuring occurred due to the heat treatment. Most of the changes (see Fig. 3 and the Appendix) occurred in the outer regions of the fuel where the prior irradiation temperature was substantially lower than the FBTA test temperature (by ≈100°C).

The irregularly shaped pores in the anisotropic α-phase structure on the fuel periphery have disappeared. An isotropic, γ-phase structure with smaller pores now prevails. The wedge-shaped crack on the fuel periphery is essentially filled with expanded fuel. The thickness of the high-density middle ring appears to have diminished and the large pores in the band just outboard of the high-density middle ring have also disappeared. The higher-temperature feature, i.e., the porous core, on the other hand, remains largely unchanged due to the similarity between the irradiation and test temperatures.

When fuel/cladding interaction occurs at higher temperatures, as in the 90-17 specimen (Fig. 6), the cladding constituents that diffuse into the fuel cause the fuel to liquefy, forming a solid/liquid two-phase mixture. This phenomenon has been seen in all previous compatibility tests conducted above the temperature for "onset of melting." In the case of 90-17, fuel liquefaction extended from the fuel/cladding interface to approximately mid-radius of the fuel, for an areal fraction of ≈70%. The region where fuel liquefaction occurred is characterized by large pores formed from the coalescence of smaller fission-gas bubbles in the fluid solid/liquid mixture. The solidified structure of the once-liquefied fuel is shown in Fig. 7. In previous tests with U-10Zr/HT9 and U-19Pu-10Zr/HT9 systems, fuel liquefaction was found to be the direct result of diffusion of the cladding components (chiefly Fe) into the fuel and lowering the fuel solidus temperature. In those tests, the liquefaction boundary was found to coincide with the Fe diffusion boundary.[8,10-11] This was confirmed also in this test series (see Section III, D). In the center of the 90-17 specimen, where Fe was absent, the condition of the fuel was essentially unchanged.

The condition of the liquid-phase-fuel/cladding interaction zone in the 90-17 specimen is illustrated in higher-magnification photomicrographs in Fig. 8. The reaction appeared to be liquid-phase (i.e., molten fuel/cladding alloy) dissolution of the cladding. On the optical photomicrographs up to 500X, the boundary separating the reacted and the unaffected cladding appeared to be smooth and well-defined. The reaction boundary had, for the most part, rounded fronts into the cladding that met in sharp ridges. There were no intergranular or intragranular cladding cracks ahead of the visible reaction boundary. The reacted cladding immediately adjacent to the reaction boundary had a dendritic two-phase appearance, indicating it was once molten. All of these features are similar to those seen in the earlier tests with U-10Zr/HT9 or U-19Pu-10Zr/HT9 fuels.[10-11]

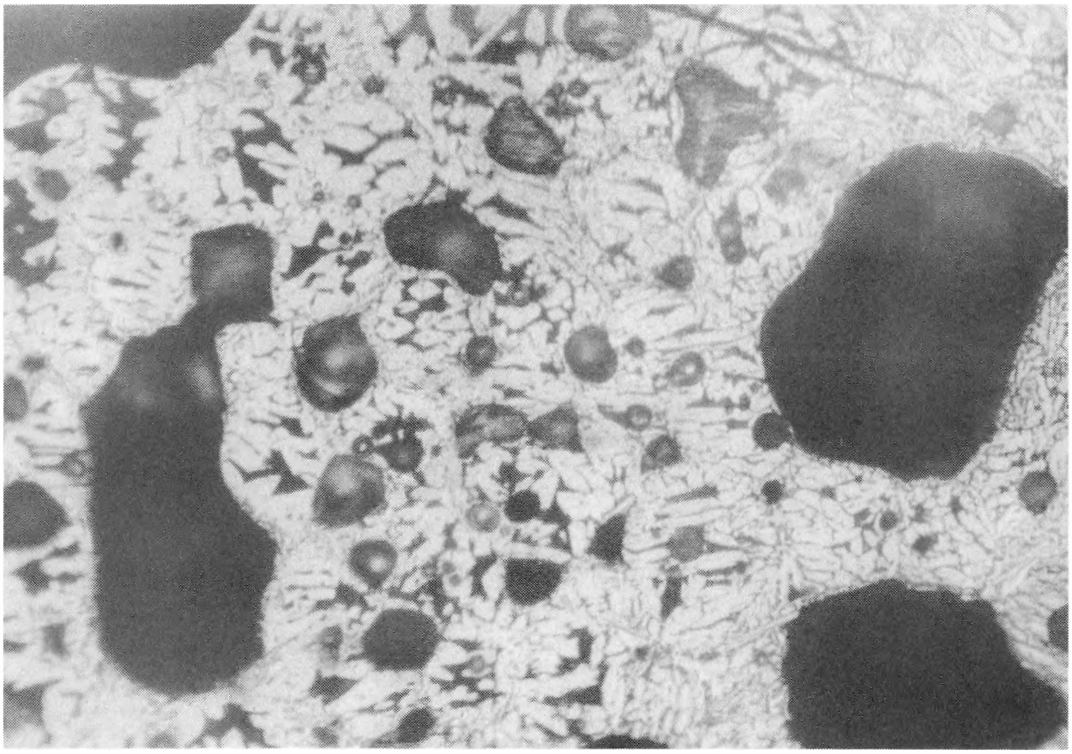

Fig. 7. Solidified Structure of Once-liquefied Fuel (500X, Etched, MCT 279082)

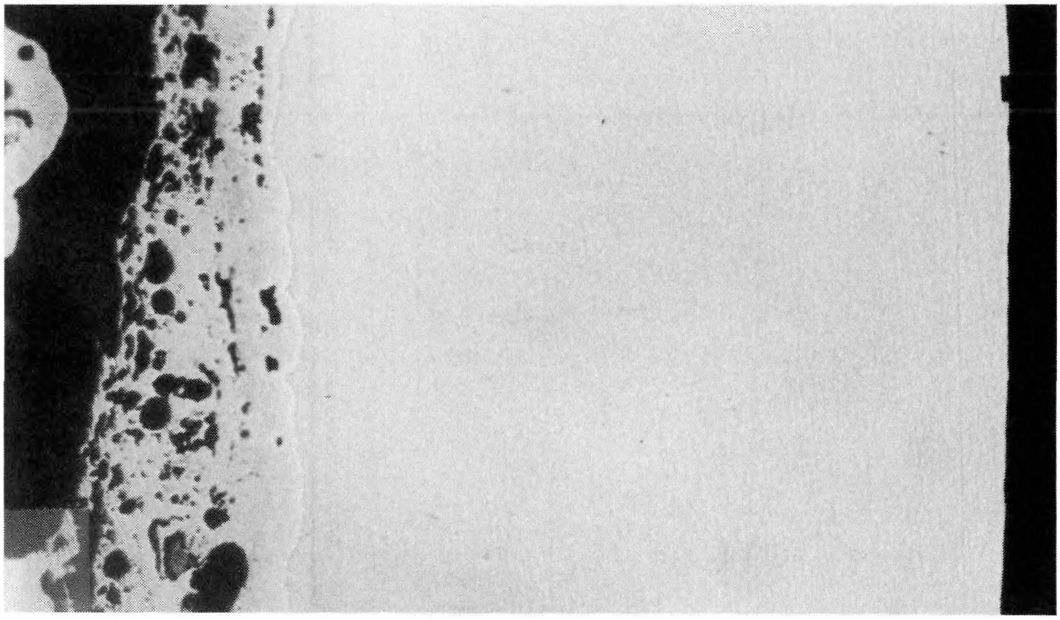

(a) 250X (As-polished, MCT 277778)

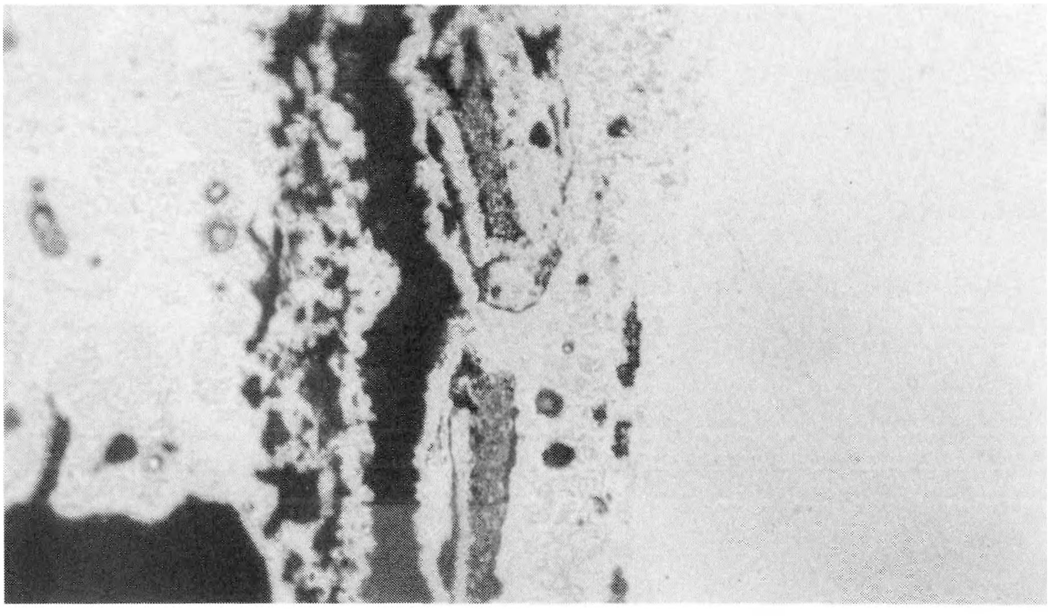

(b) 500X (As-polished, MCT 277782)

Fig. 8. Liquid-phase-fuel/Cladding Interaction in 90-17 Specimen. Unreacted cladding is at right.

## C. Cladding Penetration Rates

### 1. As a Function of Temperature

The deepest cladding penetration in the 800°C, 1.0-h, 90-17 test specimen was 55 μm, corresponding to an "effective" cladding penetration rate of $1.5 \times 10^{-2}$ μm/s. This penetration rate and the "null" rate for the 750°C, 1.0-h, 90-18 test are shown in Fig. 9, along with the existing FBTA data base. As can be seen, at both temperatures the results for the U-26Pu-10Zr/HT9 test specimens are better than those of the other metallic fuel/cladding systems previously tested. For the 90-17 test, the penetration rate is substantially below the existing empirical correlation,[8]

$$\text{Rate } (\mu\text{m/s}) = \exp\,[11.646 - 15665/T(\text{K})],$$

currently being used for design and modeling purposes.

### 2. As a Function of Time

Tests 90-19 and 90-21 were conducted with 5.0-min and 2.0-h durations, respectively, at 800°C. In conjunction with the 1.0-h 90-17 test, these three tests provided information on cladding penetration as a function of time at 800°C.

The transverse section of the 90-19 test specimen is shown in Fig. 10. Near-uniform fuel/cladding interaction occurred along essentially the entire fuel circumference in this relatively short test. The depth of liquefaction in the fuel was substantially shallower than that in the 90-17 test (Fig. 6). The areal fraction of fuel liquefaction was ≈8% and the deepest cladding penetration was 23.6 μm. The mechanism of cladding penetration was apparently the same as in the longer-duration 90-17 test, namely, dissolution by a liquid fuel/cladding mixture.

In the 2.0-h 90-21 test, with extended time for Fe diffusion into the fuel, the entire fuel cross section was affected. The transverse section of the fuel is shown in Fig. 11 and a typical section of the fuel/cladding interface is shown in Fig. 12. In spite of extended exposure to the liquefied fuel, cladding integrity was maintained. The maximum cladding penetration in the specimen was only 65.0 μm, or ≈15% of the original cladding thickness.

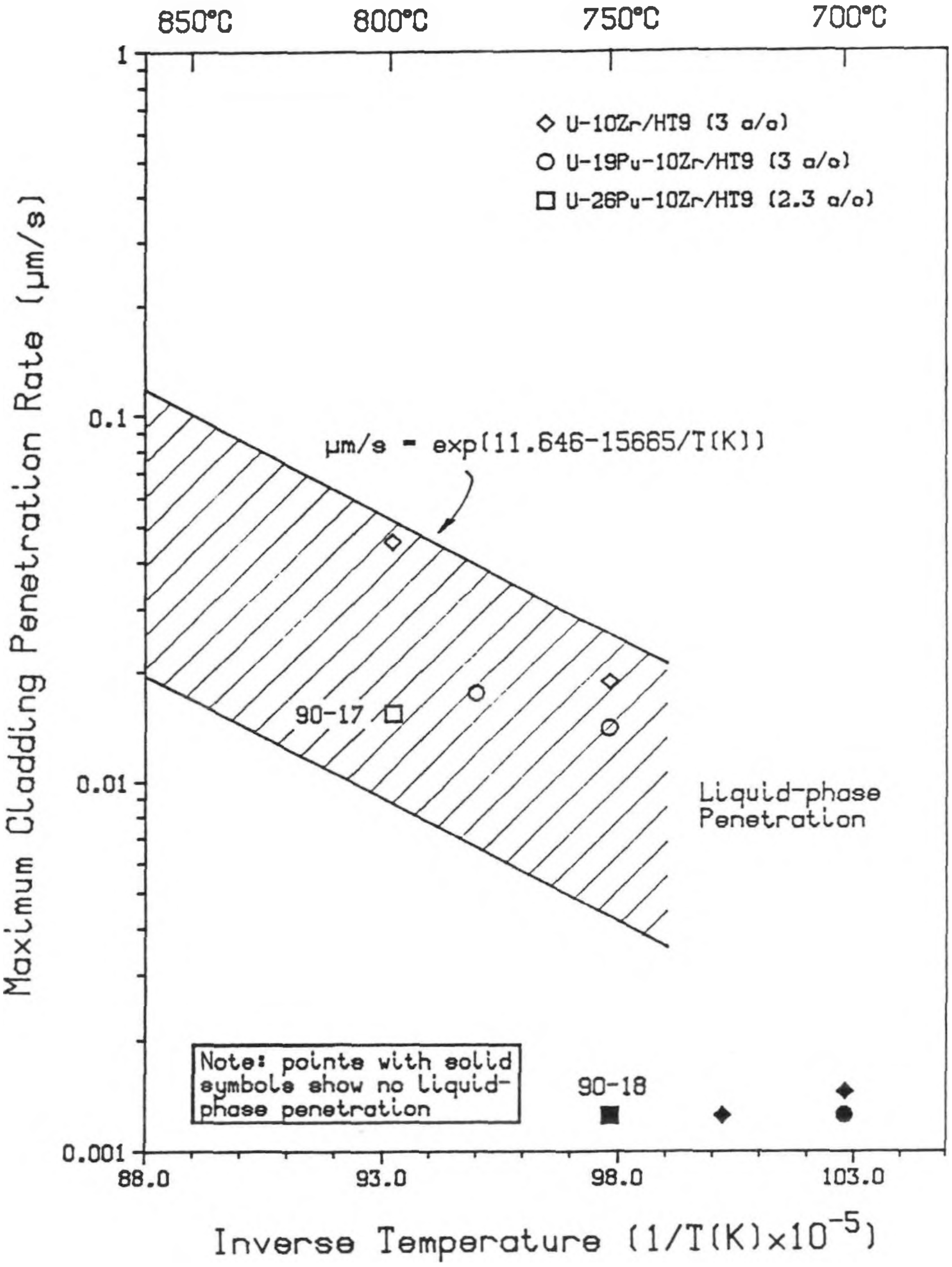

Fig. 9. Effective Cladding Penetration Rates for Specimens Tested for 1.0 h. Shaded band represents the entire FBTA data base. Specific data points for low-burnup, HT9-cladding tests are shown for comparison.

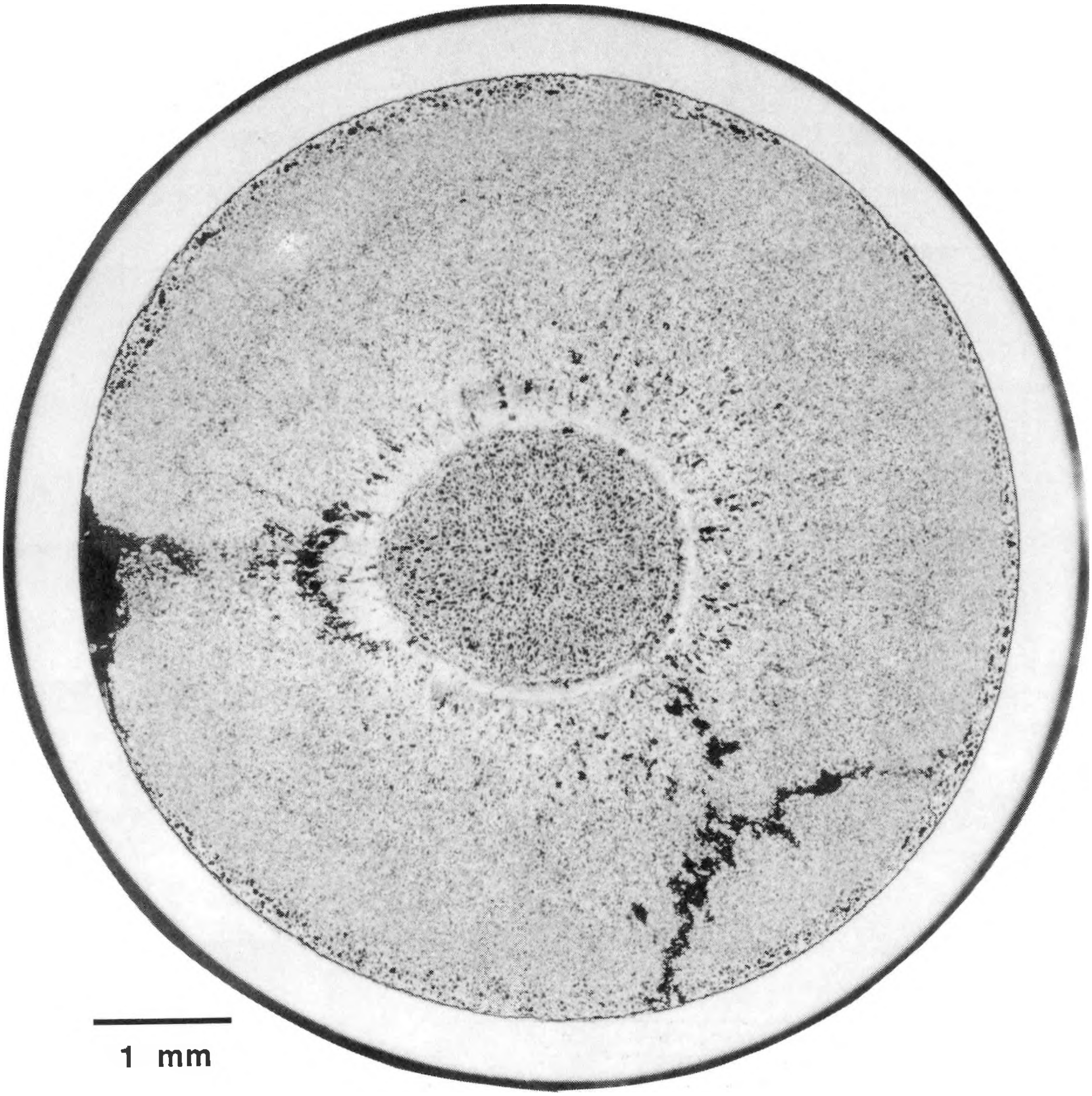

Fig. 10. Transverse Section of 90-19 Test Specimen after 5 min at 800°C. Fuel surface liquefaction was shallow. (As-polished, MCT 277873)

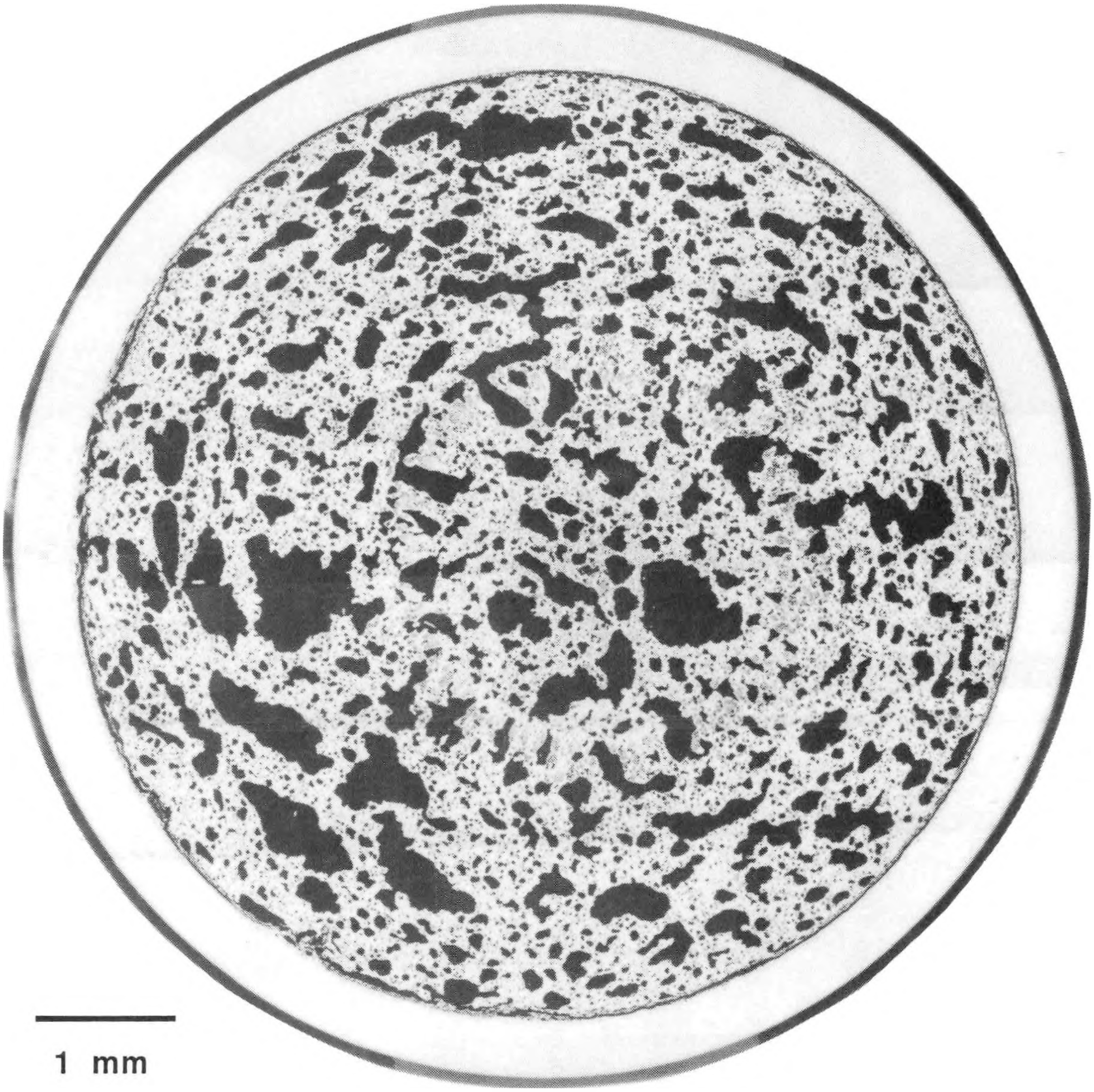

Fig. 11. Transverse Section of 90-21 Test Specimen after 2 h at 800°C. Fuel liquefaction was extended to centerline.
(As-polished, MCT 277870)

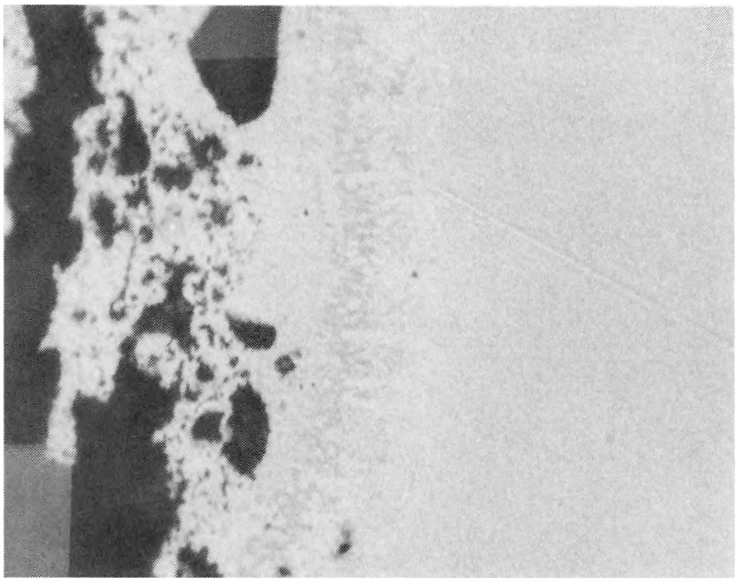

(a) 500X (As-polished, MCT 277839)

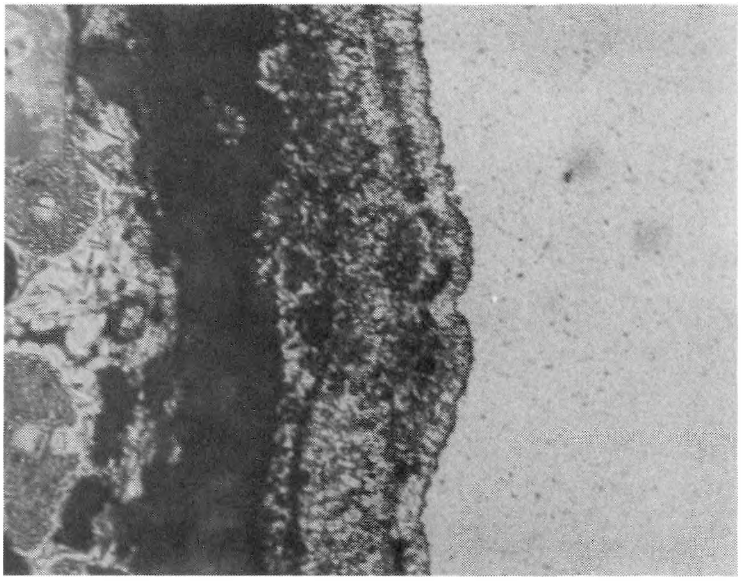

(b) 500X (Etched, MCT 278078)

Fig. 12. Typical Fuel/Cladding Interaction Zones in 90-21 Specimen. Unreacted cladding is at right.

The maximum depths of cladding penetration from the 90-17, -19, and -21 tests are plotted in Fig. 13 as a function of time. The "instantaneous" penetration of ≈20 μm at the onset of the heating cycle is likely related to the rapid melting of an interdiffusion layer formed during the steady-state irradiation, even though none was obvious (Fig. 3). After this initial rapid interaction, the rate of cladding penetration leveled off with time. This decrease in penetration rate is indicative that the reaction kinetics were probably controlled by diffusional processes across the thickening reaction layers. In Fig. 13, the behavior of the U-26Pu-10Zr/HT9 system is compared with that of the other fuel systems tested in the FBTA. In terms of cladding penetration, the behavior of the specimens in this test series is comparable to that of U-26Pu-10Zr/316SS and superior to that of U-10Zr with 316SS, D9, or HT9 cladding.

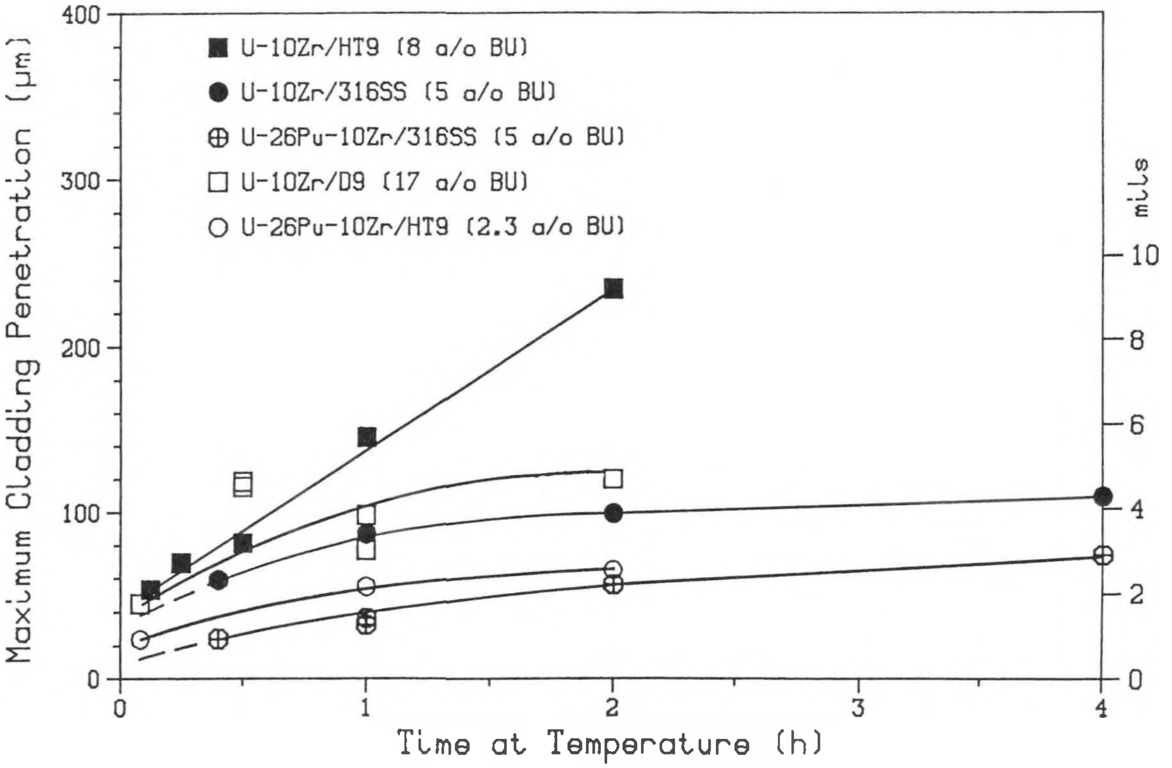

Fig. 13. Time-dependent Cladding Penetration at 800°C

## D. Fuel Behavior during NRC Bounding Event 1B

The NRC bounding event 1B is an extremely unlikely and severe event.[1] It consists of a 0.40$ UTOP, i.e., all rods withdrawn at the maximum mechanical speed, and a simultaneous loss of heat sink (LOHS). The reactor vessel auxiliary cooling system (RVACS) is assumed to be the only means to cool the reactor core during this period. In the FBTA testing, the event was simulated by a 2-min flat-top at 815°C (0.40$ UTOP) followed by a 36-h hold at 700°C (LOHS), as shown in Fig. 14.

Test 90-22, a 2-min, 815°C flat-top, was designed to investigate the separate effects of only the 0.40$ UTOP. The other three tests (90-20, -23 and -24) were conducted to investigate the combined effects of 0.40$ UTOP and LOHS. In the 90-20 and 90-23 tests, due to unanticipated weather-related AC line power interruptions, the tests were tripped at 9.3 and 16.6 h, respectively, into the planned 36-h, 700°C hold. The full 36-h hold was achieved in the 90-24 test, whose temperature history is illustrated in Fig. 14.

In the 90-22 test, even with the brief duration (2 min), fuel surface liquefaction and cladding interaction occurred, as shown in Fig. 15 (see also Fig. 19a). The extent of fuel surface liquefaction, however, was shallow and nonuniform around the circumference. The liquefied fuel/cladding reaction product apparently filled the wedged-shaped crack on the fuel periphery (about 5 o'clock in Fig. 15). Inward from the surface, the fuel microstructure was unaffected by the short test. The depth of maximum cladding penetration was ≈19 μm, which is comparable to the "instantaneous" penetration shown in Fig. 13.

In the three tests with subsequent holds at 700°C, apparently due to the sluggishness of Fe diffusion into the fuel at this modest temperature, there was no substantial additional fuel surface liquefaction during the multihour hold. This is illustrated in the transverse sections of the specimens in Figs. 16-18. However, there was noticeable further cladding penetration with time, as shown in Fig. 19. In the 90-24 specimen with a 36-h hold, the maximum cladding penetration was 121 μm, or ≈28% of the original cladding thickness. Figure 20 compares the maximum depths of cladding penetration in the four tests. The penetration rate, assuming a linear correlation, is ≈$7.9\times10^{-4}$ µm/s, or ≈3 µm/h.

While the reaction boundary appears to have the same features as in the 800°C tests, the presence of a gray phase in the middle of the reaction zone suggests a different overall reaction mechanism than that at 800°C. The morphology of this gray-phase structure is delineated in high-magnification photographs in Fig. 21. The accumulation is predominantly along a cusp-shaped boundary; root-like stringers on the fuel side and precipitated phases on the other side are also noted.

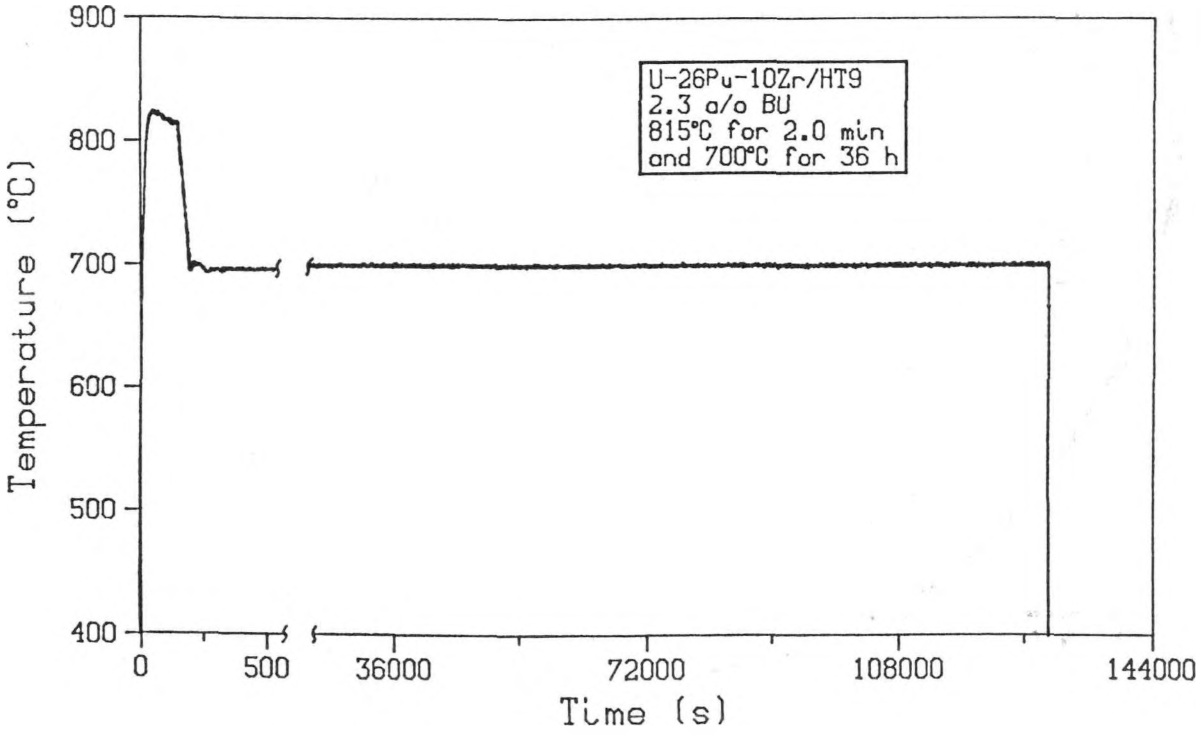

Fig. 14. Thermal History of 90-24 Test Simulating NRC Bounding Event 1B

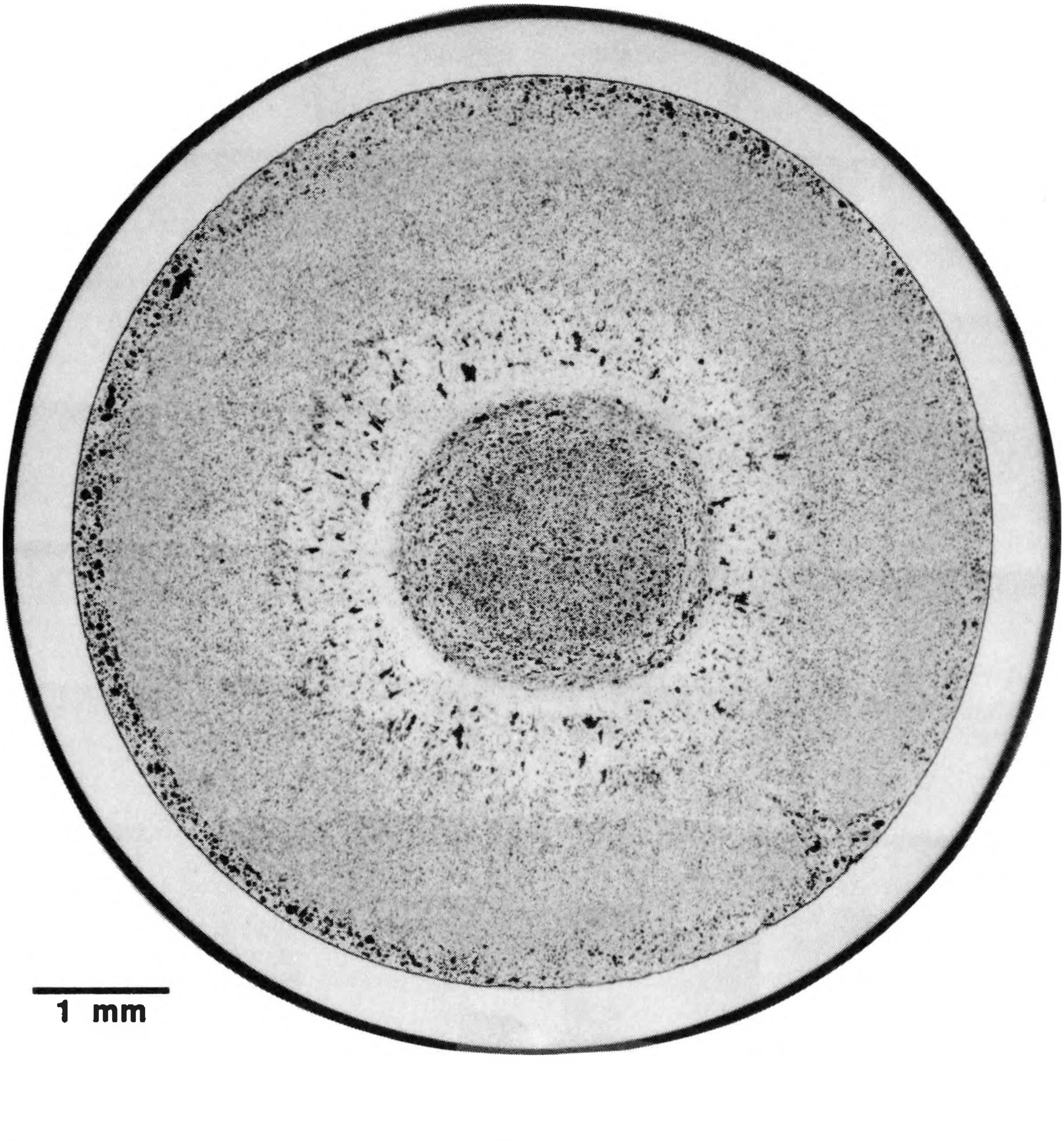

Fig. 15. Transverse Section of 90-22 Specimen after Simulated 0.40$ UTOP Event (2 min at 815°C) (As-polished, MCT 277875)

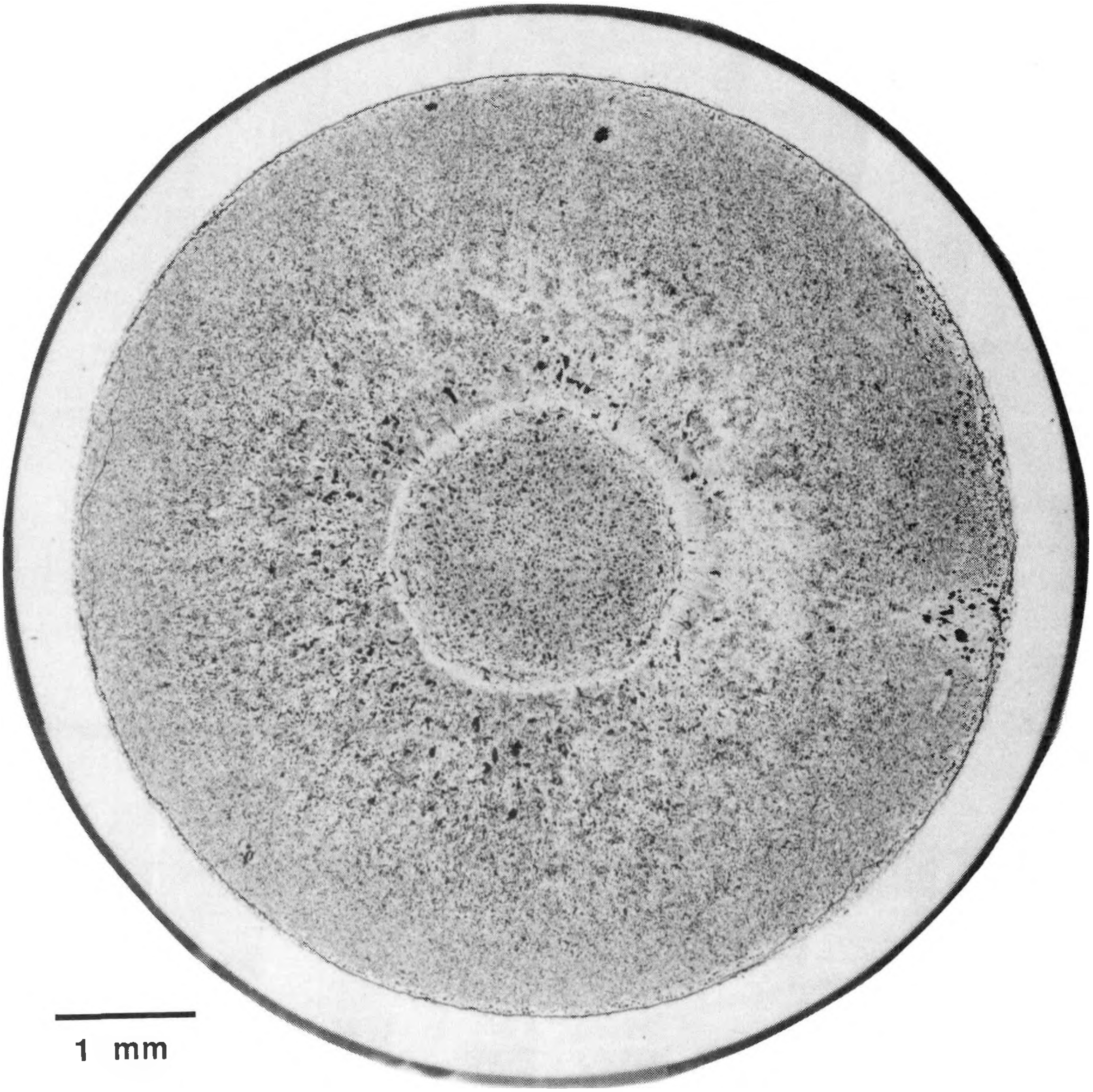

Fig. 16. Transverse Section of 90-20 Specimen after Simulated 0.40$ UTOP and 9.3-h Hold at 700°C (As-polished, MCT 277874)

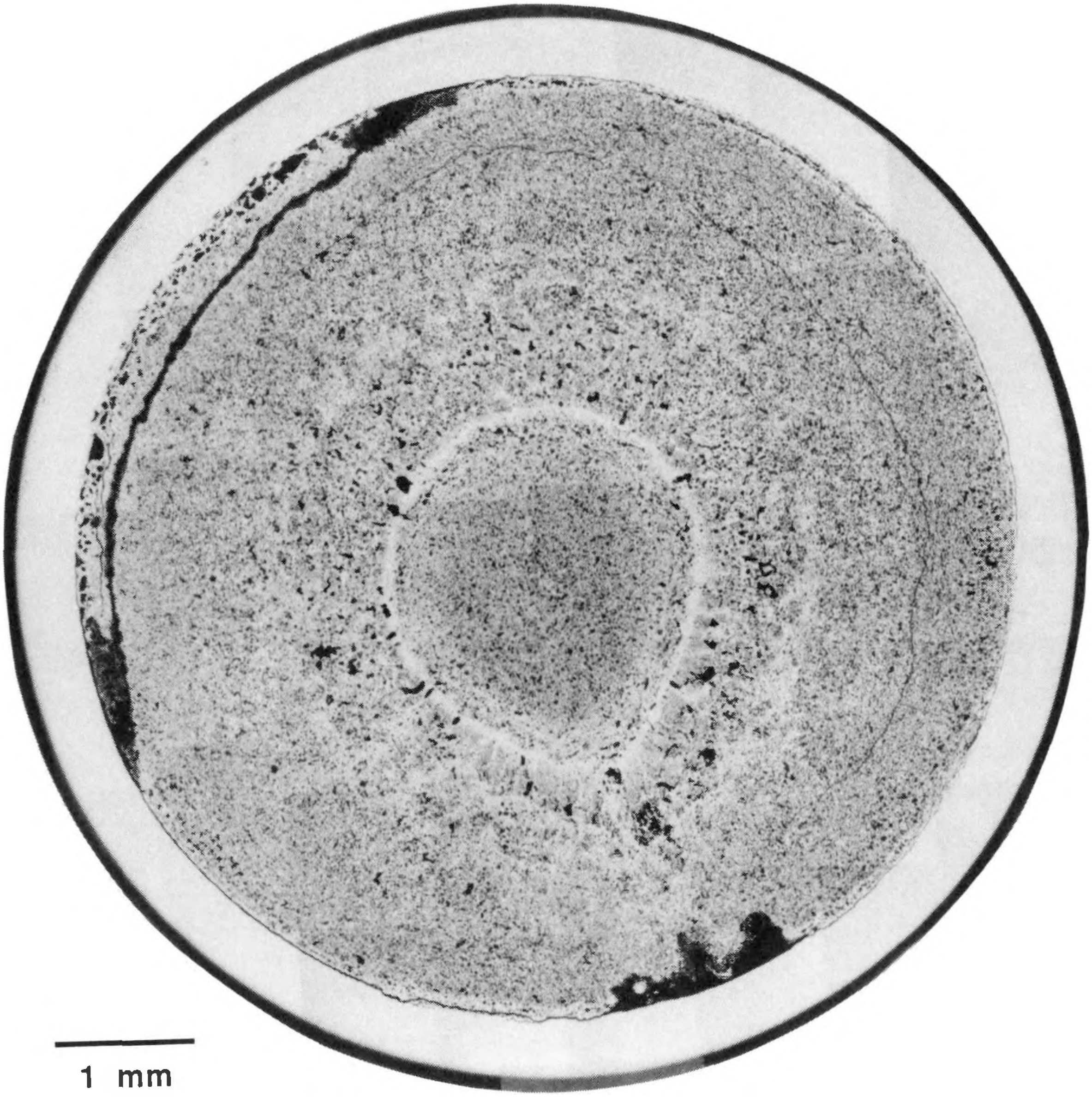

Fig. 17. Transverse Section of 90-23 Specimen after Simulated 0.40$ UTOP and 16.6-h Hold at 700°C (As-polished, MCT 277995)

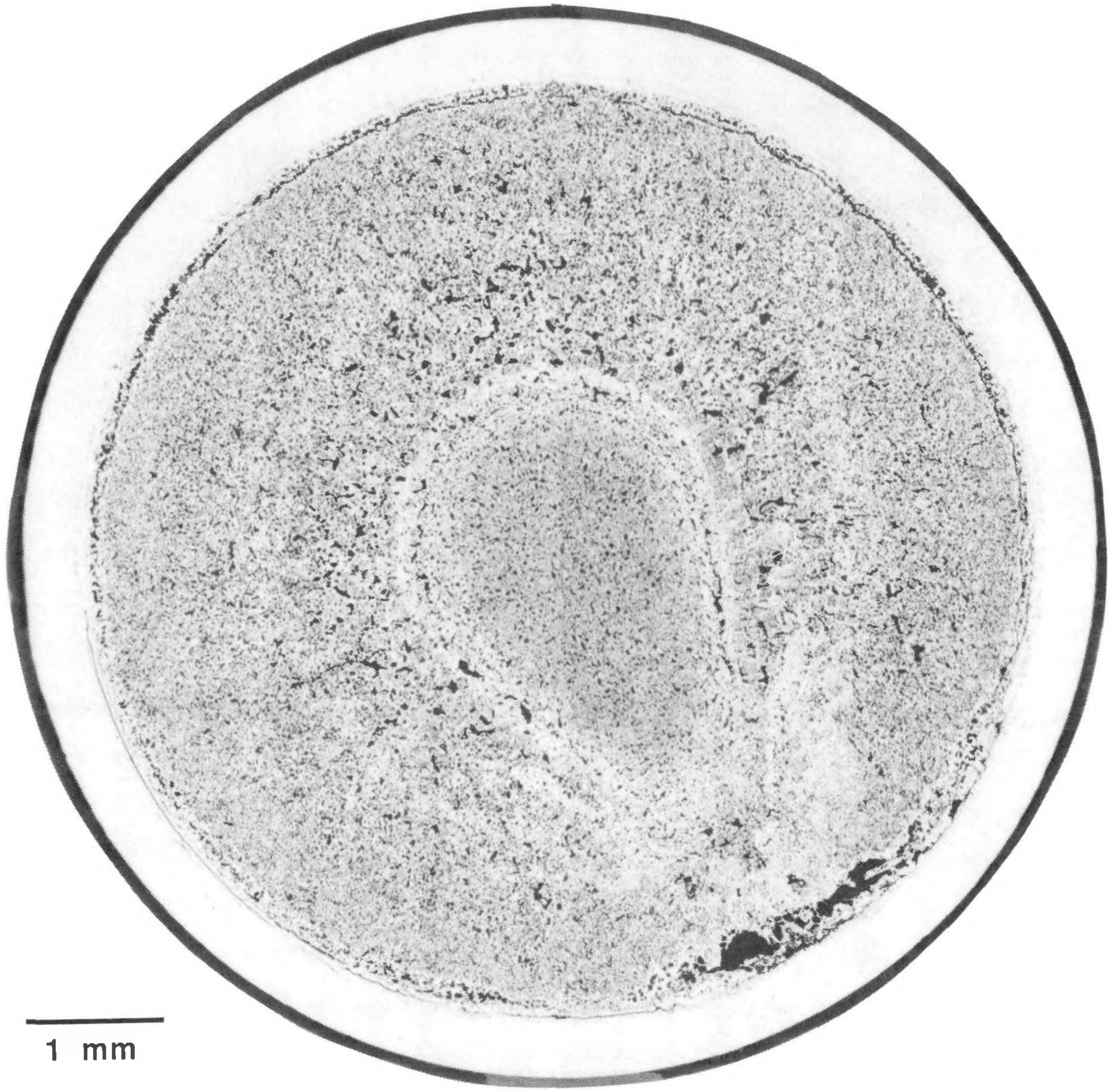

Fig. 18. Transverse Section of 90-24 Specimen after Simulated 0.40$ UTOP and 36-h Hold at 700°C (As-polished, MCT 278116)

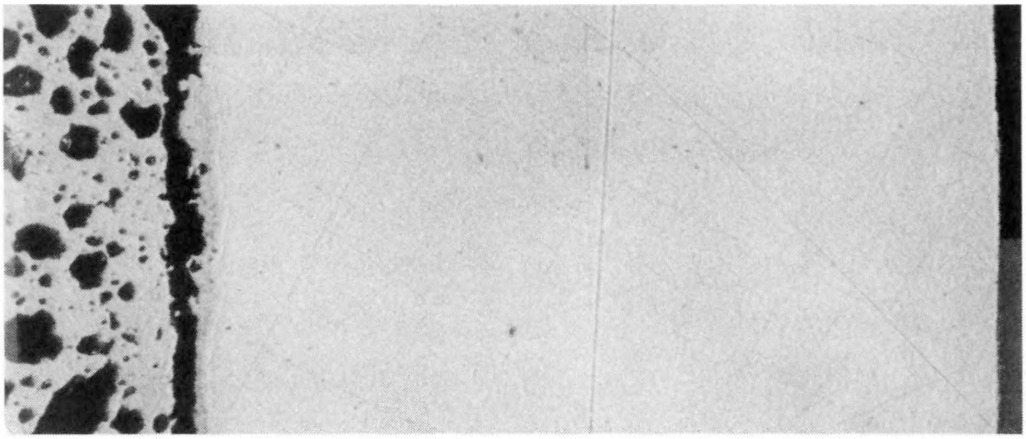

(a) UTOP only (no hold at 700°C) MCT 277844

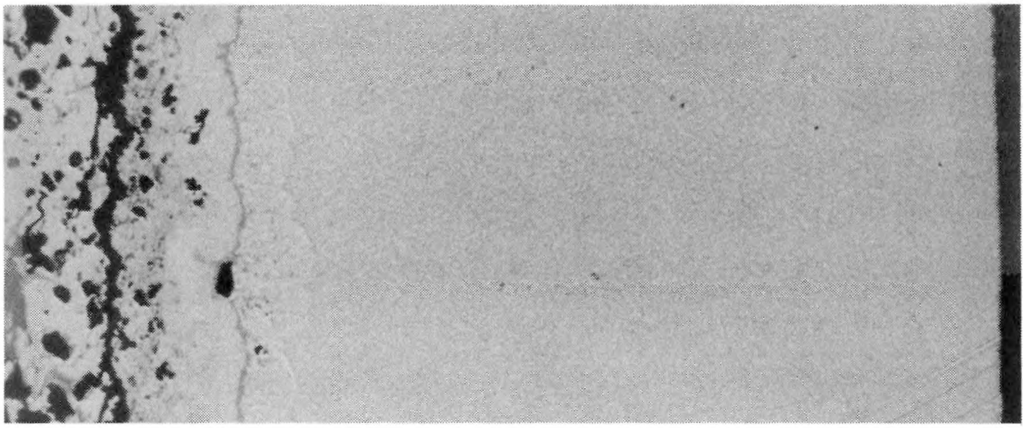

(b) UTOP and 9.3-h hold at 700°C MCT 277805

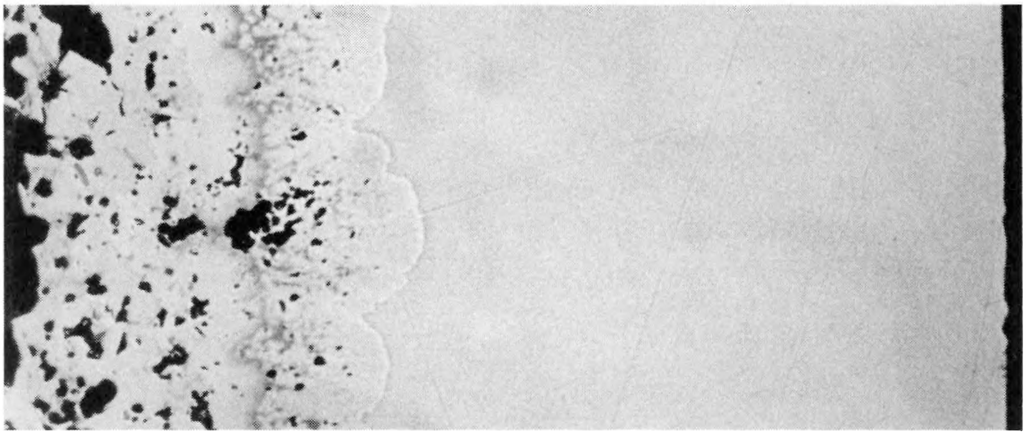

(c) UTOP and 36-h hold at 700°C MCT 278023

Fig. 19. Comparison of Fuel/Cladding Interaction in Test Specimens (a) 90-22, (b) 90-20, and (c) 90-24 (As-polished, 250X)

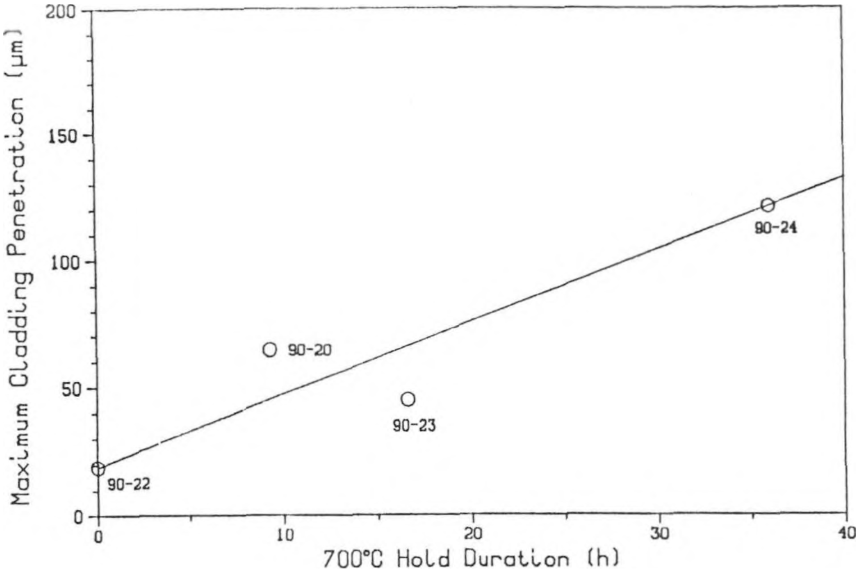

Fig. 20. Cladding Penetration during Simulated NRC Bounding Event 1B. (815°C for 2 min, followed by 700°C hold)

To investigate the reaction zone in a greater detail, a thin slice of the 90-24 test specimen was examined with a scanning electron microscope. The examined area is outlined in Fig. 22. An enlargement of this area, in backscattered electron (BSE) image, is shown in Fig. 23. [In BSE images, phases with high average atomic numbers (Z) are light, and phases with low average atomic numbers are relatively dark]. Energy-dispersive X-ray (EDX) analyses were conducted to determine the approximate compositions of the various phases. Because of the finite effective X-ray diameter (≈2-µm), the results of EDX analysis of structures whose sizes were comparable to or smaller than that of the beam tend to be less accurate due to the boundary effects from the surrounding dissimilar phases.

From Fig. 23, the following major structures were identified (from right): (A) the unreacted cladding, (B) a light gray (high-Z) band with a duplex structure, (C) the cusp-shaped band with fine stringers, (D) a dark gray (low-Z) band, (E) a medium gray band with large blocky grains, (F) reacted fuel band, and (G) unreacted fuel. The compositions of these structures, from the SEM/EDX analyses, are shown in Table III. All of these phases can be readily identified on the corresponding optical micrographs (e.g., Fig. 21).

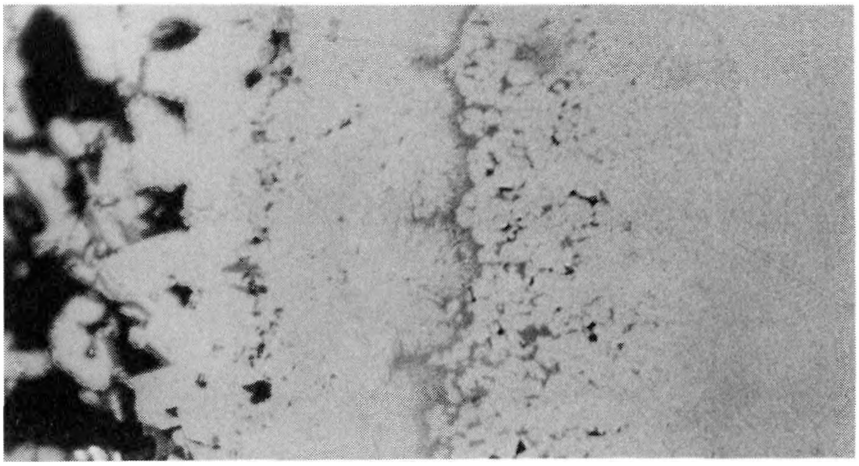

500X, As polished MCT 278025

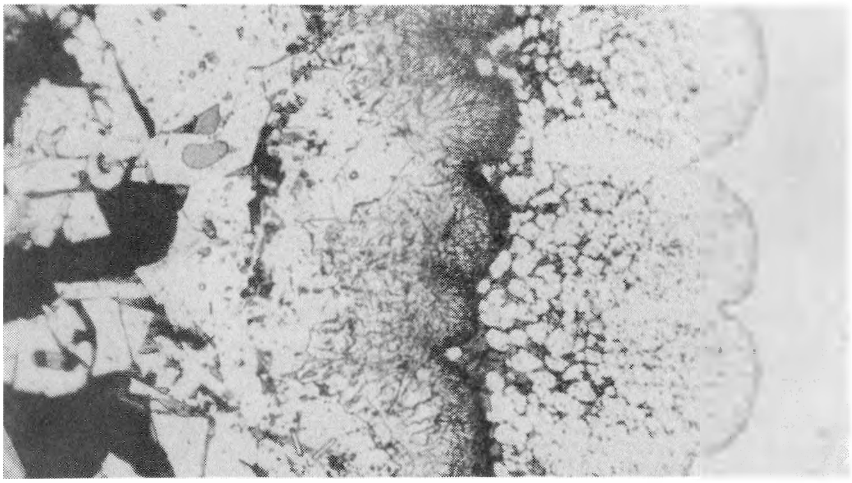

500X, Etched MCT 278088

Fig. 21. Fuel/Cladding Interaction Zone in 90-24 Test Specimen. Unreacted cladding is at right.

The composition of the unreacted cladding, both immediately adjacent to the well-defined reaction boundary and farther away, was essentially that of the original HT9 material. No diffusion-controlled subphases or intergranular penetration ahead of the visible reaction boundary could be detected on the cladding side of the boundary. (The halo seen in Fig. 23 at the reaction boundary is an electronic effect due to specimen charging.)

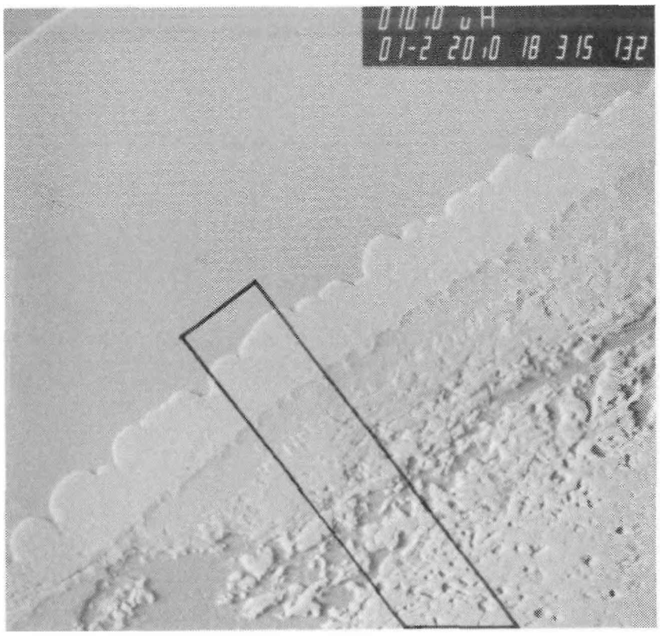

Fig. 22. Outline of Area Examined with Scanning Electron Microscope. Cladding OD can be seen at upper left.
MCT 315132

Table III. SEM/EDX Compositions (at.%) of Fuel/Cladding Interface Zones in FBTA 90-24 Specimen

| Zones[a] | | U | Pu | Zr | Fe | Cr |
|---|---|---|---|---|---|---|
| A. | Cladding away from interface | - | - | - | 87 | 13 |
| | Cladding adjacent to interface | - | - | - | 87 | 13 |
| B. | Gray phase (bulk) | 35 | 13 | 3 | 41 | 8 |
| | Lighter gray intergranular phase | 43 | 35 | - | 19 | 3 |
| C. | Stringer structure[b] | 14 | 13 | 39 | 25 | 9 |
| D. | Dark-gray band | 2 | 1 | 54 | 33 | 10 |
| E. | Medium-gray band | 16 | 7 | 50 | 24 | 3 |
| F. | Reacted fuel, adjacent to Zone E | 47 | 36 | 14 | 3 | - |
| G. | Unreacted fuel | 48 | 34 | 18 | - | - |

---

[a] Letters refer to the areas shown in Fig. 23.

[b] Due to the small particle size, reported composition is the local area average, i.e., includes the background.

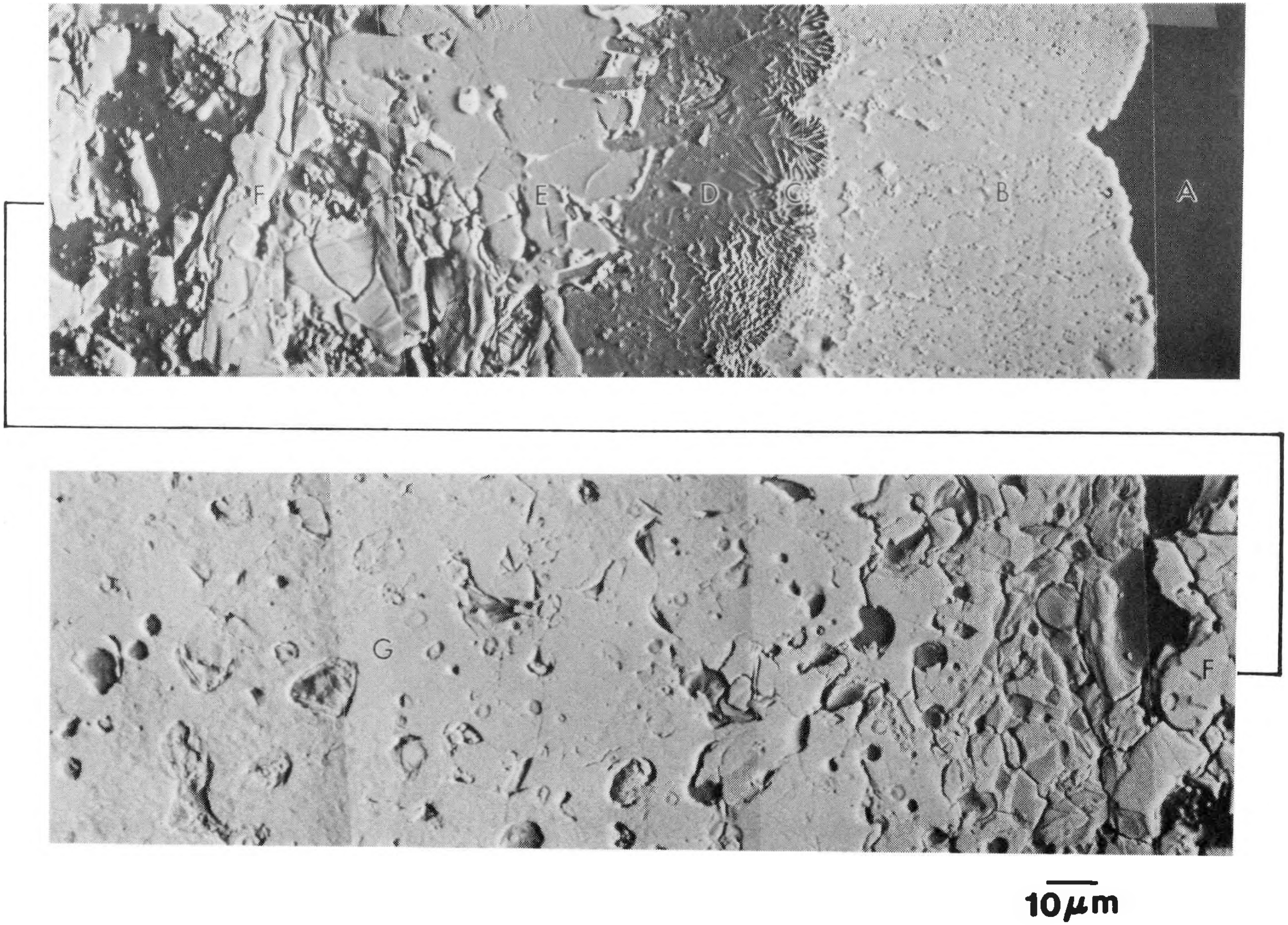

Fig. 23. BSE Image of Outlined Area in Fig. 22. From right: (A) the unreacted cladding, (B) a light gray (high-Z) band with a duplex structure, (C) the cusp-shaped band with fine stringers, (D) a dark gray (low-Z) band, (E) a medium gray band with large blocky grains, (F) reacted fuel band, and (G) unreacted fuel. MCT 278463

The reaction band immediately adjacent to the intact cladding has a two-phase structure (see Fig. 23, Area B): a gray phase interspersed with a small amount of lighter gray phase. The lighter gray phase, shown in a higher magnification in Fig. 24, appears to be a grain-boundary structure and is more abundant away from the cladding interface. The composition of the gray phase determined by EDX is essentially uniform throughout the band: ≈48 at.% (U+Pu), ≈49 at.% (Fe+Cr), and only a trace of Zr. That of the light gray, grain-boundary phase is ≈78 at.% (U+Pu) and ≈22 at.% (Fe+Cr). Because the two phases are interspersed and have small particle sizes, even with careful spot selection, it is likely that the EDX data for the gray phase contains contribution from the light-gray phase, and vice versa. Within the accuracy of the data, it appears that the gray phase contains the $(U,Pu)Fe_2$ intermetallic compound, whereas the light-gray, grain-boundary phase may be rich in the $(U,Pu)_6Fe$ compound. According to the U-Pu-Fe ternary equilibrium diagram, the material in this region would have been a solid/liquid mixture with an overall composition on the Fe-rich side of eutectic at the test temperature (700°C during the 36-h hold). During cool-down at the end of the test, additional $(U,Pu)Fe_2$ precipitated by nucleating on the inside wall of the remaining cladding, followed by solidification of the lower-melting $(U,Pu)_6Fe$ (i.e., the rejected lighter-gray phase on the grain boundaries).

Area D in Fig. 23 is a dark-gray, dense band consisting of essentially all Zr and Fe (Cr) (see Table III). According to the equilibrium phase diagram,[14] the material is probably an intermetallic compound between Zr and Fe (Cr). Because all Zr-(Fe,Cr) compounds have high solidus temperatures (>900°C), this phase was apparently a solid at the test temperature. Evidence of its crystalline growth inward during the test can be seen in Fig. 23. Because the U and Pu constituents from the fuel must diffuse through this solid band to react with the cladding, the band was probably an effective barrier in controlling the overall rate of fuel/cladding interaction.

The stringers (Area C, Fig. 23) on the cladding side of this band appear to be a fuel-rich phase, although the composition could not be accurately determined due to its small particle size. Based on the grayness on the BSE images (see Fig. 24), the stringers appear to have a composition similar to that of the intergranular phase in band B. Within the cusps, the orientations of the stringers are predominantly perpendicular to the cusps. The stringers are probably a diffusion-induced subgrain structure, along which much of the U and Pu fuel constituents migrated to the reaction front. Similar structures have been noted in an unirradiated U-19Pu-10Zr/HT9 diffusion-couple specimen after 300 h at 725°C.[5] The formation mechanism of the stringers and the cusp-shaped morphology is not known at this time.

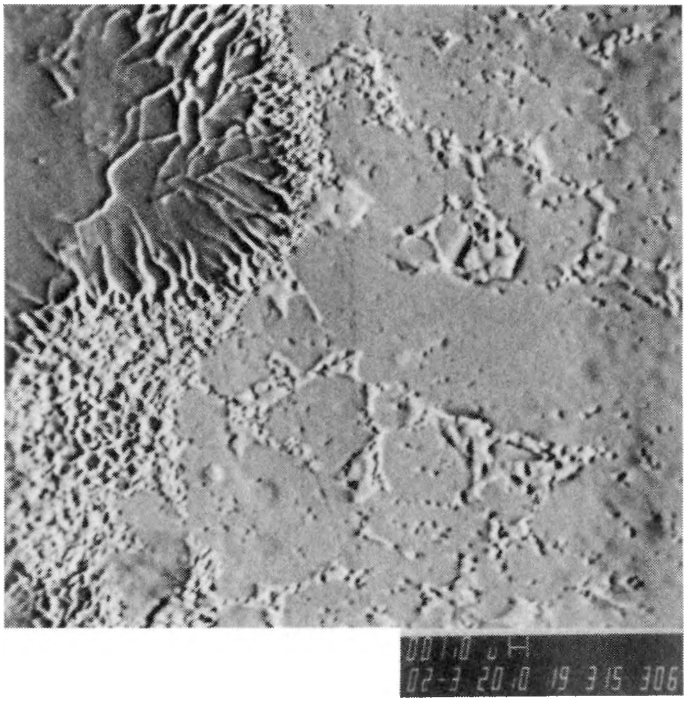

Fig. 24. BSE Image of Interface Region between Areas B and C, Showing Grain-Boundary Structure in Area B and Stringers in Area C. See Fig. 22 for area definition.

Area E in Fig. 23 is also a high-Zr, high-Fe (Cr) phase, but with a substantially greater concentration of (U, Pu) than in Area D (see Table III). It appears to be a different intermetallic compound than that in Area D because the demarcation between the two areas is sharp and distinct. A high-Z (light gray) phase is found on some of the grain or subgrain boundaries in this band.

Further inward was the reacted fuel phase (Area F in Fig. 23); the thickness of the band is ≈100 μm. The concentration of Fe, which is responsible for the reaction, is small (≈3 at.% max.) and decreases with radial position in this band. Extensive fracturing indicates that the reacted material is brittle. Beyond this band, there is no detectable Fe and the microstructure of the fuel appears to be unchanged from the test.

## IV. DISCUSSION

### A. Effects of Pu Content in Fuel

U-Pu-Fe phase-relations data[12] and results of differential thermal analysis experiments[13] both suggested inferior fuel/cladding compatibility with increasing Pu content in the fuel. A lower liquid-phase formation temperature than those in the U-10Zr and U-19Pu-10Zr fuel systems was thus expected. Likewise, the rate of cladding penetration was anticipated to be higher for the U-26Pu-10Zr fuel in this test series.

The FBTA results, however, showed the compatibility behavior of the U-26Pu-10Zr fuel to be somewhat better than that of the lower Pu-content fuels. This seemingly contradictory result underscores the fact that the FBTA tests are kinetic studies and, as such, are strongly affected by fuel/cladding interfacial conditions. The factors that affect the interfacial conditions include as-cast fuel surface structure, steady-state diffusional layers, and the reaction-product layers that form during the high-temperature interaction. The phase-diagram studies and DTA experiments, on the other hand, represent equilibrium conditions that likely could not be attained in transients or in tests with finite durations, i.e., minutes to hours. Because the FBTA tests employ irradiated fuel specimens with prototypical fuel/cladding interfaces, and because the test durations are comparable to those of the in-reactor off-normal events, the data from FBTA tests are considered to be more applicable than the equilibrium data for analyzing or predicting in-reactor fuel/cladding compatibility behavior.

## B. Penetration at the Onset of Heating

In the two short-duration tests (90-19, 5 min, 800°C; and 90-22, 2 min, 815°C), the "instantaneous" cladding penetration was ≈20 μm in both cases. This suggested rapid liquefaction of a layer in the cladding ID that was affected by steady-state interdiffusion, even though such a layer was not identified metallographically. (A diffusion-affected layer, however, was identified with an electron microprobe in a prior U-10Zr/HT9 specimen[11] that also showed a rapid cladding penetration at the onset of heating.) For most short transients, e.g., PPS-terminated events, much of the cladding wastage would probably be due to this "instantaneous" penetration, provided the fuel/cladding interface temperature exceeds the liquid-phase formation temperature. If not, the likelihood of any effective cladding wastage would be slight. It should be emphasized that the rate correlation shown in Fig. 8 is applicable only for over-temperature events with a duration of approximately 1 h.

## C. Fuel Compaction

In the 90-21 test (Fig. 10), the fuel was extensively liquefied at 800°C and yet maintained a stable foamy structure at the end of the 2-h test. There was little fuel runout from the open ends of the specimen. This suggests that a compaction of the gas-entrapped molten phase into a high density mass - a potential reactor safety concern - is highly unlikely.

## D. Long-duration Test Potential with the FBTA

Until this test series, the longest duration employed in FBTA tests was 7.0 h, i.e., approximately the length of a normal work day. In this test series, operation of the FBTA overnight without attendance was carried out for the first time. With the use of hardware and software trip protection built into the system,[6] all three overnight tests were safely conducted. Two of the three tests (90-20 and 90-23) were terminated unexpectedly due to weather-related AC line power failures. In both cases, the built-in trip protection mechanisms performed as designed and brought the FBTA system to a safe shutdown. There were no losses of data or damage to equipment in either test. Throughout the extended testing period, specimen temperature control was impeccable. The potential for using the FBTA system to conduct longer-term tests was substantially strengthened.

## V. SUMMARY

1. No detectable liquid-phase-fuel/cladding interaction occurred in the U-26Pu-10Zr/HT9 (2.3 at.% burnup) specimen tested at 750°C for 1.0 h. This threshold temperature is somewhat better than that of other metallic fuel systems previously tested.

2. At higher temperatures, fuel/cladding interaction would cause liquefaction of the fuel surface and liquid-phase cladding attack.

3. The rate of cladding attack is substantially below the existing rate correlation. There is no apparent rate increase due to the higher Pu content in the fuel.

4. As in the other irradiated fuel systems tested in the FBTA, a shallow surface layer in the cladding ID may liquefy rapidly at the onset of the heating. This surface layer is probably formed by fuel/cladding interdiffusion during the steady-state irradiation.

5. In terms of time-dependent cladding penetration, the behavior of the specimens in this test series is comparable to that of U-26Pu-10Zr/316SS and superior to that of U-10Zr with 316SS, D9, or HT9 cladding.

6. During a concurrent UTOP and LOHS event (NRC Event 1B), the cladding was slowly attacked during the 700°C hold. The maximum cladding wastage was 121 μm, or ≈28% of the original cladding thickness.

## VI. ACKNOWLEDGMENTS

This work was performed under the auspices of the U.S. Department of Energy. The authors wish to thank L. A. Neimark of Argonne's Materials and Components Technology Division for many valuable discussions, R. G. Pahl of EBR-II for providing the irradiated test fuel pins, the competent staff at Argonne's Alpha-Gamma Hot Cell Facility for conducting the tests and metallographic examination, and E. L. Hartig and C. A. Malefyt for preparing and editing the manuscript.

## VII. REFERENCES

1. Dubberley, A. E., et al., "Design for Passive Safety in The ALMR," International Fast Reactor Safety Meeting, pp. 131-142, Snowbird, UT (August 1990).

2. Marchaterre, J. F., et al., "Integral Fast Reactor Concept Inherent Safety Features," ASME Winter Meeting, CONF-86-1211-24, *86-WA/NE-14*, Anaheim, CA (December 1986).

3. Chang. Y. I., "The Integral Fast Reactor," *Nucl. Tech.*, *88*, 129-138 (November 1989).

4. Zegler, S. T., and Walter, C. M., "Compatibility Between U-Pu-based Fuels and Potential Cladding Materials," AIME Nuclear Metallurgy Symposium on Plutonium Fuels Technology, AIME *13*, pp. 335-344 (October 1967).

5. Hofman, G. L., et al., "Chemical Interaction of Metallic Fuel With Austenitic and Ferritic Stainless Steel Cladding," International Conference on Reliable Fuels For Liquid Metal Reactors, pp. 4.121-4.131, Tucson, AZ (September 1986).

6. Tsai, Hanchung, "A Versatile Apparatus For Studying The Behavior of Irradiated Fuel," 37th Conference on Remote Systems Technology, pp. 88-93, San Francisco, CA (November 1989).

7. Kramer, J. M., Argonne National Laboratory, personal communication (1990).

8. Tsai, Hanchung, "Fuel/Cladding Compatibility in Irradiated Metallic Fuel Pins at Elevated Temperatures," International Fast Reactor Safety Meeting, pp. 257-267, Snowbird, UT (August 1990).

9. Kramer, J. M., Argonne National Laboratory, personal communication (1990).

10. Tsai, Hanchung, et al., "Compatibility of Low-Burnup U-10Zr Fuel with HT9 Cladding at Elevated Temperatures," Argonne National Laboratory Report ANL-IFR-104 (February 1989).

11. Tsai, Hanchung, Argonne National Laboratory, unpublished data (1990).

12. Leibowitz, L., "Phase Relations for Fuel-Cladding Interactions," Argonne National Laboratory Report, ANL-IFR-54 (October 1986).

13. Leibowitz, L., et al., "Compatibility of U-Pu-Zr Alloy Fuel with Stainless Steel Cladding," Argonne National Laboratory Report ANL-IFR-109 (July 1989).

14. Hausen, M. and Anderko, K., Constitution of Binary Alloys, Second Ed., Genium Publication Corp., Schenectady, New York (August 1986).

# APPENDIX: CONDITION OF AS-IRRADIATED T678 PIN BEFORE FBTA TESTING

## A. Summary of HFEF NDE and Gas Sampling Results

### 1. Visual Examination

No unusual features.

### 2. Pin Weighing

No significant change between the preirradiation weight (213.22 g) and post-irradiation weight (213.19 g).

### 3. Neutron Radiography

No unusual features. Fuel zone formation and wedge-shaped cracking on fuel surface is noticeable. Fuel column lift-off at the base is ≈3 mm. See Fig. A1.

### 4. Cladding Profilometry

Spiral contact profilometry showed negligible cladding strain. See Fig. A2.

### 5. Plenum Gas Sampling

The amount of gas collected in the pin plenum was $2.4 \times 10^{-3}$ mole, of which 86% was fission gas (Xe and Kr). If 0.25-mole fission-gas generation per mole of fission is assumed, the amount of collected fission gas corresponds to a release fraction of 88% from the fuel matrix.

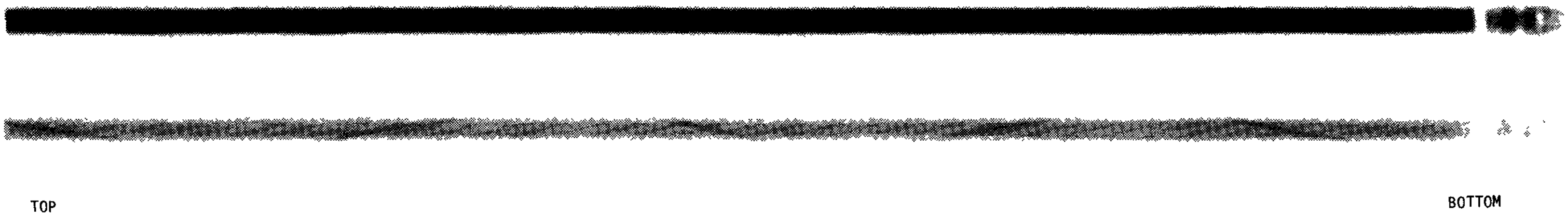

Fig. A1. Neutron Radiographs of T678 at Two Different Exposures

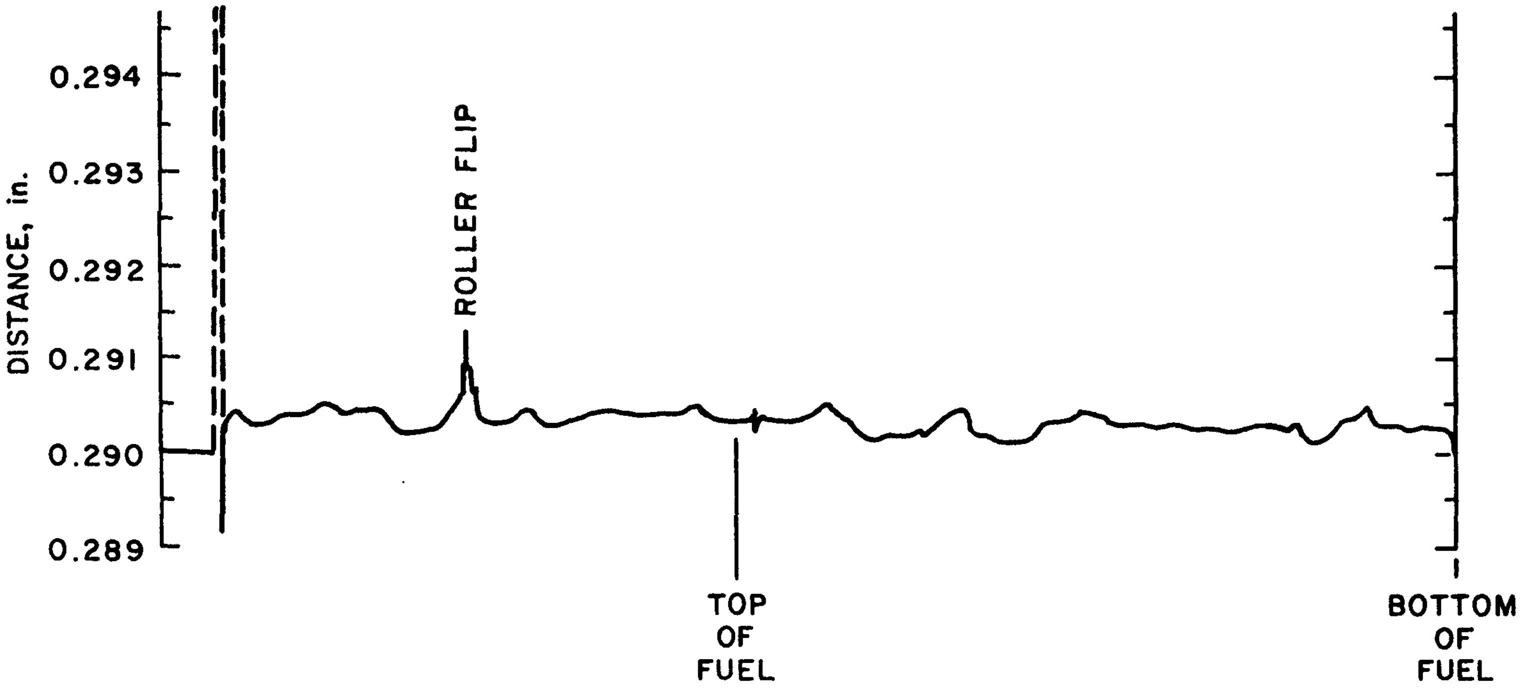

Fig. A2. Contact Profilometry Trace of Pin T678, Showing Negligible Cladding Strain

## B. Summary of Metallographic Examination Results

Four transverse sections of the as-irradiated fuel were metallographically examined. The axial locations (X/L) of the four sections, denoted M1 through M4, were 0.20, 0.49, 0.77 and 0.91, respectively. The photocomposites of the M1, M2, and M4 sections are shown in Figs. A3-A5; that for the M3 section (X/L = 0.77) is given in Fig. 3.

Fuel swelling, due to gaseous fission-product buildup, had effectively closed the as-built fuel/cladding gap. Gap closure was less complete at the M1 section, however, due to the lower-temperature, lower-power operation. At the three higher elevations with higher operating temperature and power, the fuel formed distinct concentric zones because of the redistribution of U and Zr during irradiation. At the M1 section, zone formation was only at an embryonic stage. With the M2 section as an example, the identifiable zones are (from center, see Fig. A4): (1) a porous core, (2) a dense middle ring with largely columnar grains, (3) a transitional zone with a dense fuel matrix but large pores, (4) a wide band with more-uniformly distributed porosity, and (5) an anisotropic periphery with large irregularly-shaped pores. These features, though not fully matured due to the relatively low fuel burnup, are typical for irradiated metallic fuels with a high Pu content.

A wedge-shaped crack in the fuel periphery was noted in the M2, M3 and M4 sections. (These cracks were also seen in the FBTA test specimens.) Formation of these cracks was apparently associated with the anisotropic swelling of the fuel early in life. Such anisotropic swelling is more pronounced in fuels with high Pu content. The void space in the crack was beginning to be filled by the swollen fuel at the fuel surface constrained by the cladding. At a later stage (i.e., high burnup), the crack would likely be fully filled.

In spite of the relatively low burnup, deposits of solid fission products were noted in the fuel, mostly in the fuel zone immediately inward of the porous fuel periphery, at an r/R of ≈0.6-0.7. Figure A6 shows some of the typical deposits found in sections M2 and M3. Based on past experience, these deposits consist mainly of lanthanide fission products.

It should be pointed out, however, that there was little noticeable fission-product accumulation on or near the fuel surface. (Lanthanide fission products on the fuel surface or in the fuel/cladding gap may degrade fuel/cladding compatibility.[8]) Deposition of fission product precipitates in the porous central zone or the dense middle ring was also minimal.

The condition of the HT9 cladding at all four elevations appeared to be excellent. There were no obvious indications of fuel/cladding chemical interaction as a result of the steady-state irradiation. Figure A7 shows typical fuel/cladding interface areas from sections M3 and M4. The slight gap (≈15 μm average) between the fuel and cladding at room temperature was apparently from reactor shutdown, i.e., due to the fuel/cladding differential thermal contraction. At irradiation temperature, the gap was probably closed.

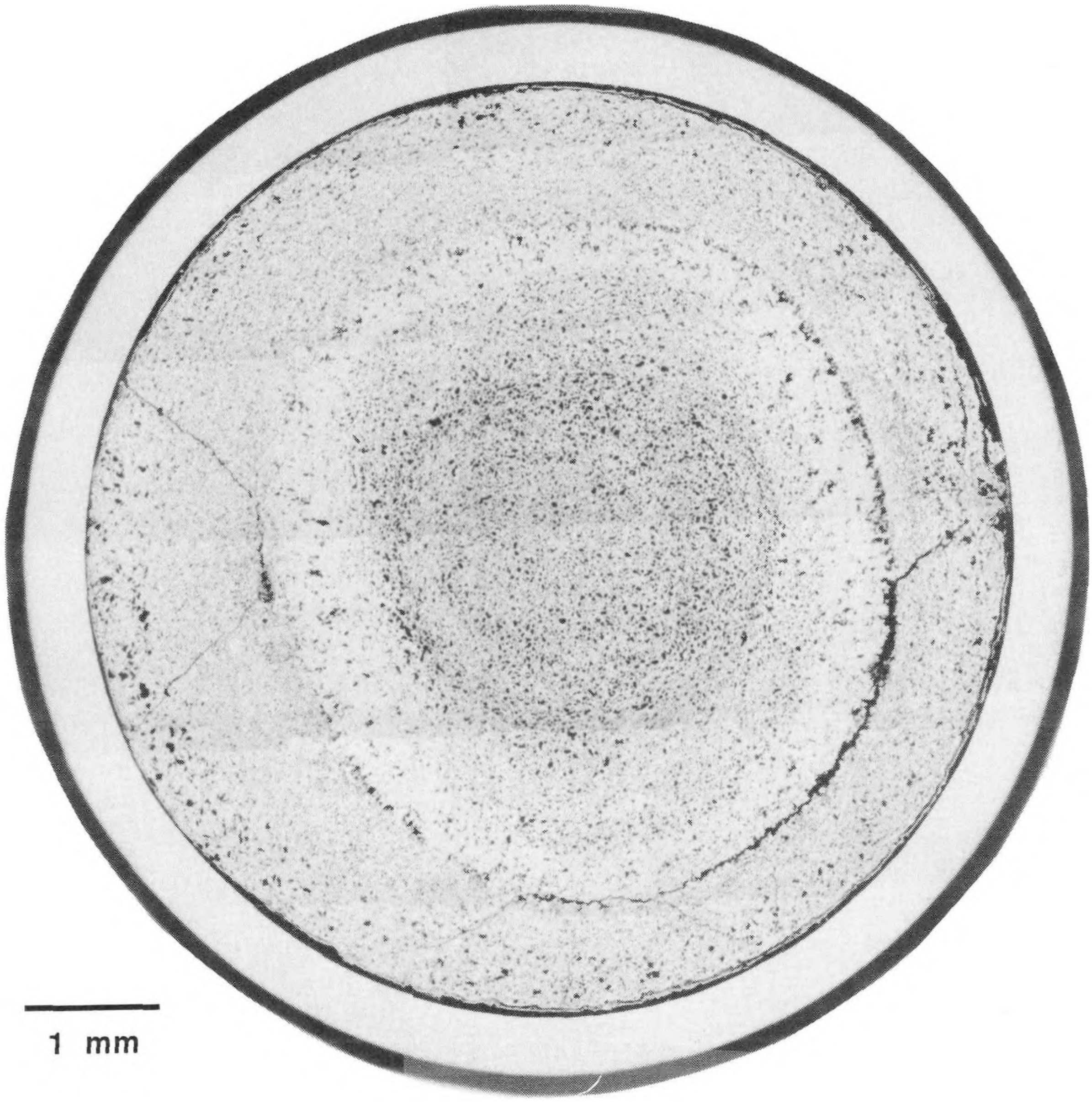

Fig. A3. Transverse Section of Pin T678 at X/L = 0.20 (M1) after Steady-state Irradiation (As-polished, MCT 277590)

Fig. A4. Transverse Section of Pin T678 at X/L = 0.49 (M2) after Steady-state Irradiation (As-polished, MCT 277591)

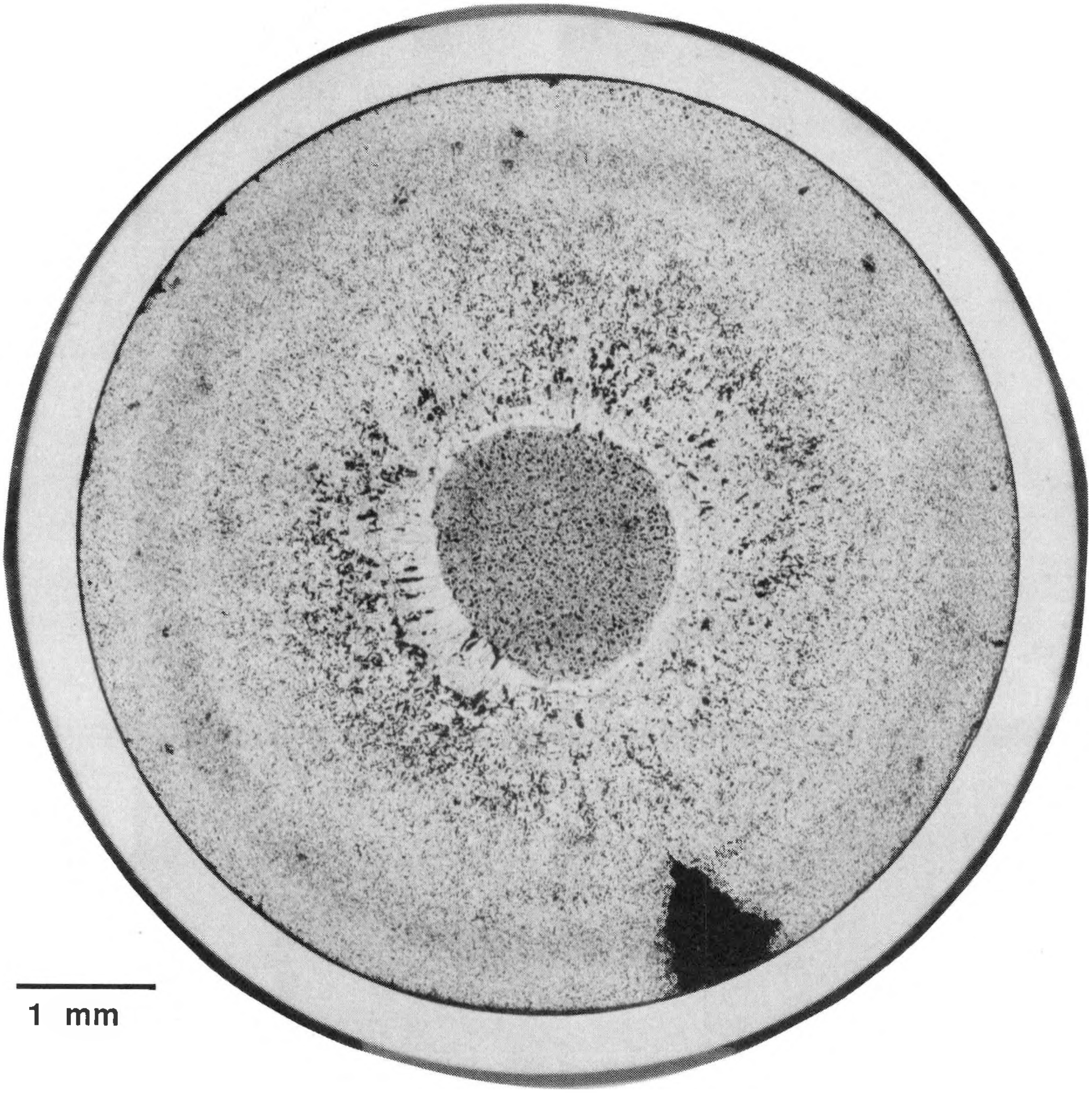

Fig. A5. Transverse Section of Pin T678 at X/L = 0.91 (M4) after Steady-state Irradiation (As-polished, MCT 277593)

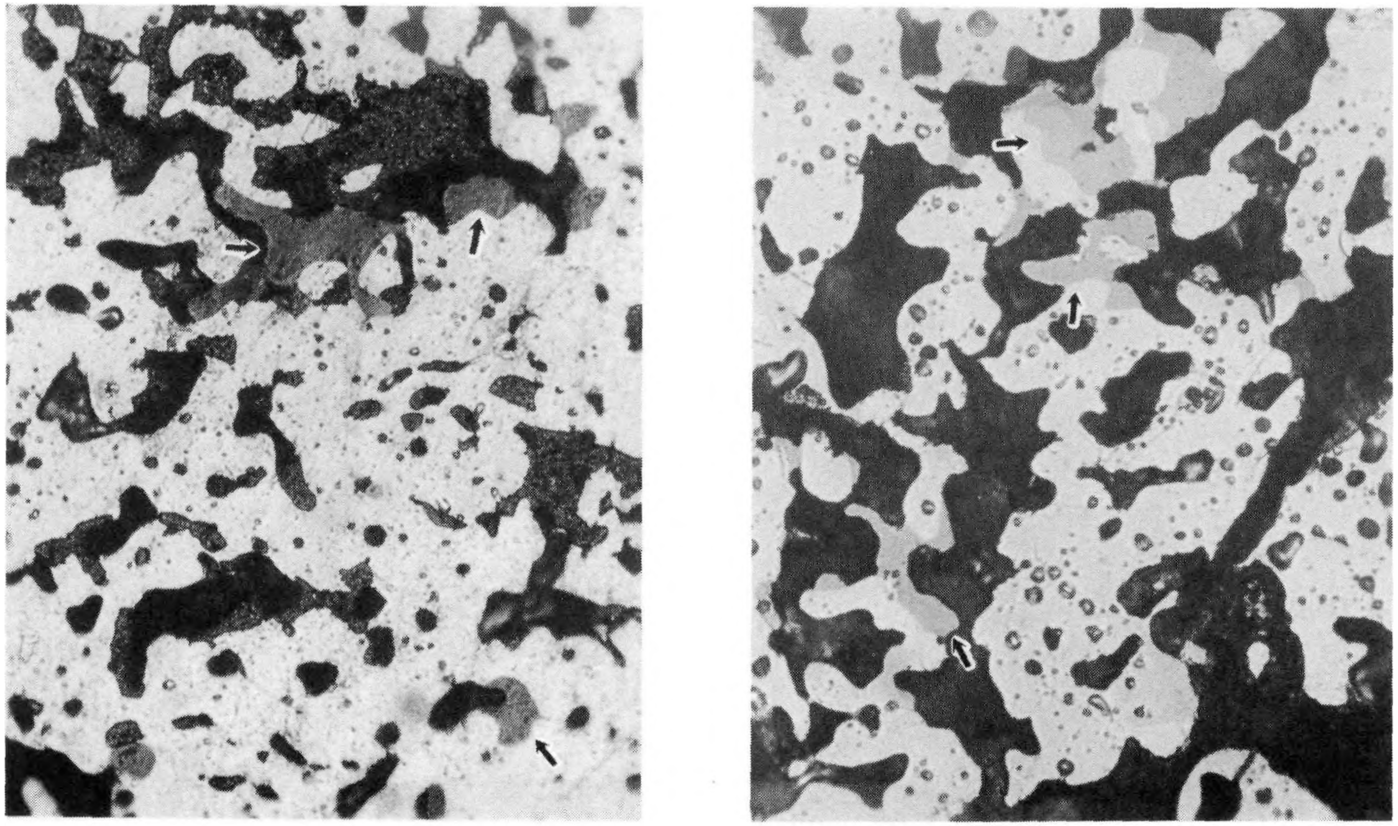

Section M2
(MCT 277726, 500X, AP)

Section M3
(MCT 277668, 500X, AP)

Fig. A6. Fission-product Accumulations in As-irradiated Fuel

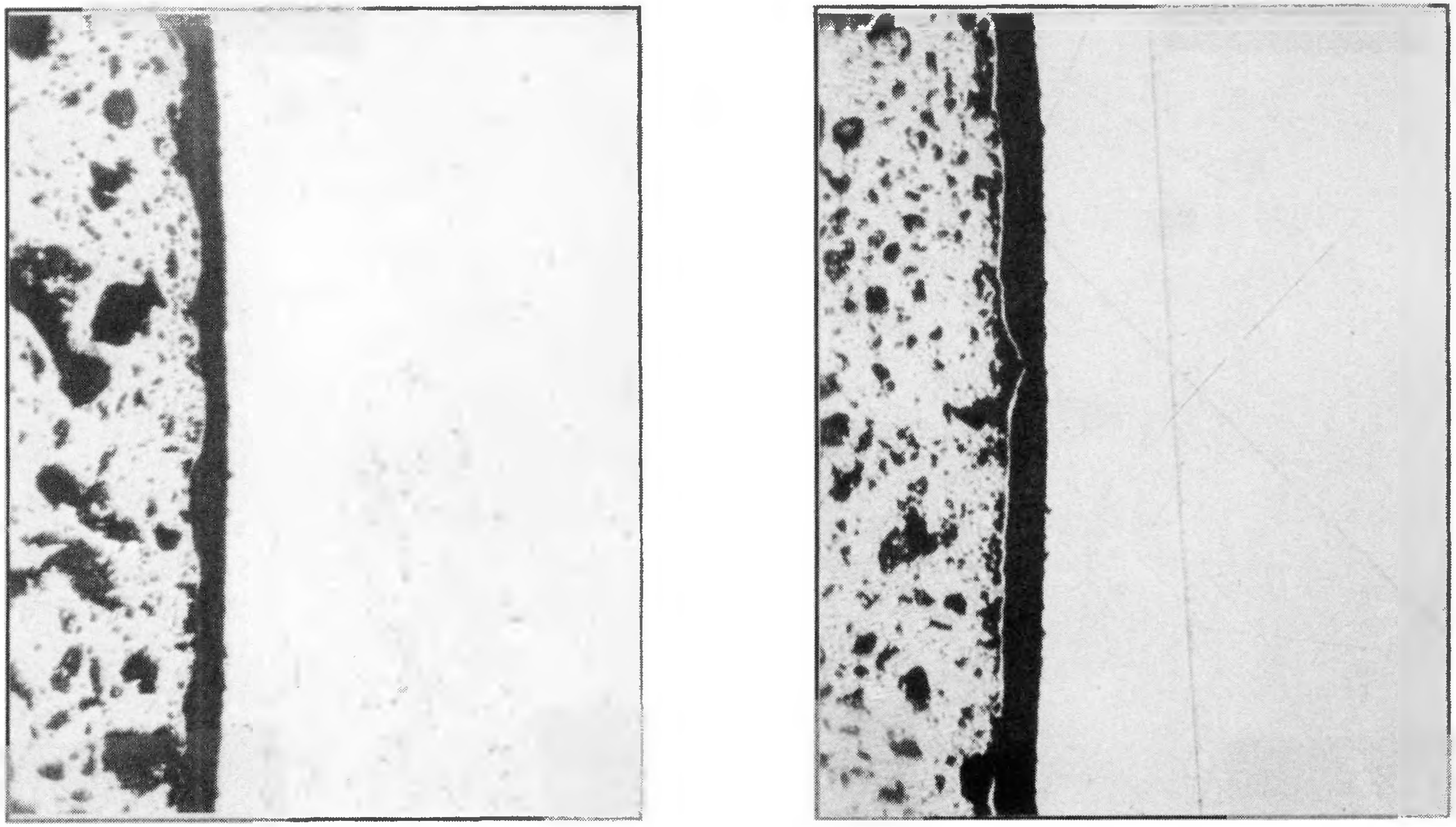

Section M3, X/L = 0.77
(MCT 277760, 250X, AP)

Section M4, X/L = 0.91
(MCT 277695, 250X, AP)

Fig. A7. As-irradiated Pin T678 Cladding, Showing No Obvious Fuel/Cladding Interaction